Algorithm Theoretical Basis Document (ATBD)

version 3.0, 15 September 2021

Contents

Author	Approved	Signature	Date
Marcello Passaro, and Algorithm Development Team	Ellis Ash		15 September 2021
ESA Acceptance			

Issue	Date	Comments
1.0	8 July 2019	First version submitted for ESA approval
1.1	7 November 2019	Updates following review by ESA
2.0	27 May 2020	Updates for year 2 of the project
3.0	15 September 2021	Updates for year 3 of the project

List of Acronyms

ACDC   Amplitude Compensation and Dilation Compensation
ADP   Algorithm Development Plan
ALES   Adaptive Leading Edge Subwaveform
ATBD   Algorithm Theoretical Basis Document
BH   Brown-Hayne (model)
cci   Climate Change Initiative
DC   Dilation Compensation
DD   Delay-Doppler
DtC   Distance to Coast
E3UB   End-to-End ECV Uncertainty Budget
ECV   Essential Climate Variable
EMF   Empirical Model Function
FFT   Fast Fourier Transform
GC   Geometric Corrections
GCCM   Grey-level Co-occurrence Matrices
GDR   Geophysical Data Record
GTS   Global Telecommunication System
L4   Level 4
LR-RMC   Low Resolution with Range Migration Correction
LRM   Low Rate Measurement
LUT   Look-Up Table
MAD   Median Absolute Deviation
MLE   Maximum Likelihood Estimator
MQE   Mean Quadratic Error
NM   Nelder Mead (algorithm)
NRCS   Normalized Radar Cross-Section
OSTST   Ocean Surface Topography Science Team
PHCP   Percentage of High Correlation
PLRM   Pseudo Low Rate Measurement
PTR   Point Target Response
PVASR   Product Validation and Algorithm Selection Report
RA   Radar Altimeters
RMC   Range Migration Correction
RR   Round Robin
R.m.s.   Root mean square
RMSE   Root mean square error
S3A   Sentinel-3A
S3B   Sentinel-3B
SAR   Synthetic Aperture Radar
SGDR   Sensor Geophysical Data Records
SI   Scatter Index
SSH   Sea Surface Height
SSP   Sea State Processor
STD   Standard Deviation

SWH   Significant Wave Height
WHALES   Wave Height Adaptive Leading Edge Subwaveform (retracker)
w.r.t   with respect to
WV   Wave (mode for SAR)

1. Introduction

This document presents the Algorithm Theoretical Basis Document (ATBD) for **Sea_State_cci**, deliverable 2.2 of the project. This is version 3, produced as an update to version 2.0 in the second year.

The objective of this document is to define the Algorithm Theoretical Basis for all the algorithms developed in the framework of the SS_cci project and taking part in the Round Robin exercise described in the Product Validation and Algorithm Selection Report (PVASR). These algorithms include processings for Low Resolution Mode (LRM) Altimetry, Delay-Doppler (DD) Altimetry and Synthetic Aperture Radar (SAR). Subsequent sections present the algorithms for these elements in turn.

2. Algorithms for Satellite Altimetry (Low Resolution Mode) Processing

2.1 ATBD-1: WHALES

2.1.1 Function

The Low Resolution Mode (LRM) waveforms are characterised by a rising leading edge that becomes less steep as the SWH increases, and a slowly decreasing trailing edge. The advent of the Adaptive Leading Edge Subwaveform (ALES, Passaro et al. 2014)) retracker has already showed the way to keep the quality of the retrievals in the open ocean while improving the data quality and quantity in the last ~25 km from the coast, where waveforms are particularly corrupted by heterogeneous backscattering from land and sheltered water. Nevertheless, besides still using the full echo to retrieve parameters that are located on the leading edge, the standard retracking method is still affected by a suboptimal distribution of the residuals in the fitting process, which results in high level of noise in the estimations.

WHALES is designed as a unified way to solve these and other problems currently affecting the standard product, and is based on three principles:

1) The application of a weighted fitting solution, whose weights are adapted to the SWH in order to guarantee a more uniform distribution of the residuals during the iterative fitting. This guarantees significantly more precise estimations.

2) A subwaveform strategy to focus the retracking on the portion of the signal of interest, avoiding heterogeneous backscattering in the trailing edge (partially inherited from the ALES retracker). This guarantees efficiency in the coastal zone and a better representation of the oceanic scales of variability.

3) The decorrelation between SWH and sea level estimation, which corrects for possible covariant errors and increases furthermore the precision.

Moreover, a revisiting of the look-up tables used to correct for the Gaussian approximation of the Point Target Response in the Brown model ensures that the accuracy in the estimation is tailored to the new retracking solution.

2.1.2 Algorithm Definition

INPUT:
- Waveform data: Sensor Geophysical Data Record (SGDR)
- Mission
- Instrumental Correction
- Weights

OUTPUT:
- SWH
- σ_0
- Quality Flag

MATHEMATICAL STATEMENT:

WHALES is a two-pass retracker. The retracking of each waveform follows the procedure described in the following flow diagram:
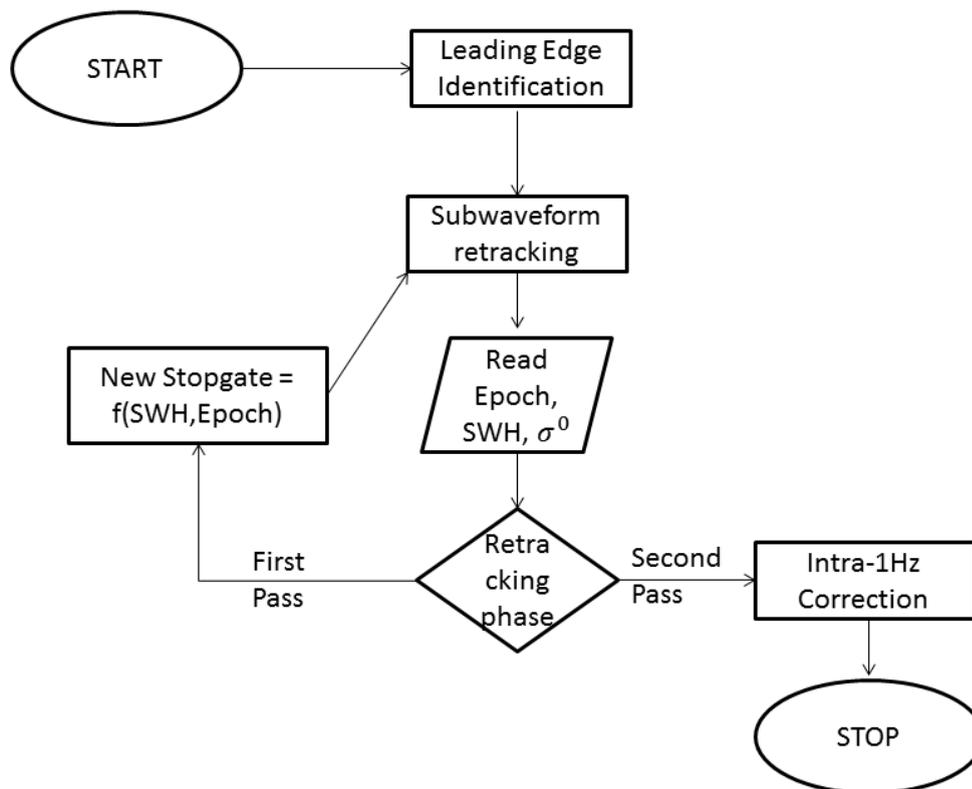
Figure 1: Flow diagram of WHALES

The functional form used to fit the real waveforms is the Brown-Hayne model as described in the following section. The original waveforms of any altimeter mission are discretized in elements called "gates". In WHALES, the first gate number is identified as 0 and the x-axis of a waveform is sampled in time. For example for Jason-3:

$$x = [0, 1 * \tau, 2 * \tau..., 103 * \tau]$$

Where τ is the spacing between two consecutive gates in time (3.125 ns in Jason-3).

The Leading Edge identification includes also the normalisation of the waveform and is performed following these substeps:

---

1) The waveform is normalised with normalisation factor N, where N = 1.3 * median(waveform)

2) The leading edge starts when the normalised waveform has a rise of 0.01 units compared to the previous gate (startgate)

3) At this point, the leading edge is considered valid if, for at least four gates after startgate, it does not decrease below 0.1 units (10% of the normalised power).

4) The end of the leading edge (stopgate) is fixed at the first gate in which the derivative changes sign (i.e. the signal starts decreasing and the trailing edge begins), if the change of sign is kept for the following 3 gates.

The scope of the normalisation is indeed to take as reference power a value close to the maximum of the leading edge and, in the case of oceanic waveforms with standard trailing edge noise, the proposed factor N is a good approximation.

The first pass of WHALES involves a subwaveform that goes from startgate to stopgate+1. It is therefore a leading-edge-only subwaveform retracking. The vector of weights is filled with 1s. The convergence is therefore found by means of an unweighted Nelder-Mead estimator (see next section). The unknowns and the corresponding initial conditions applied are:

$$\tau = startgate - 1; \; \sigma_c = (stopgate - startgate)/(2 * \sqrt{2}); \; P_u = 2 * mean(D[startgate:stopgate])$$

Where D is the normalised waveform. In case convergence is not reached, a new attempt is performed extending the subwaveform by two gates, until convergence or until the waveform limit.

After the first pass, the WHALES coefficients are applied to extend the subwaveform. As explained in the next section, the issue is one of defining an appropriate new stopgate for the second pass retracking based upon the SWH estimates from the first pass. For Jason-3, the following coefficients are used:

Stopgate = Ceiling(Tracking point + 3.89 + 3.86*SWH)

These coefficients were recomputed specifically for the current purposes as explained in the section 2.1.4 "WHALES Coefficients".
Using the new limits of the subwaveform, a second NM estimation is performed using the same initial conditions of the first pass. This time, the SWH estimation of the first pass is also used to identify the proper set of weights (see next section). WHALES therefore is adaptive in both the subwaveform width and the weights.

The SWH estimated in the second pass is instrumentally corrected by means of a look-up table that takes into account the bias due to the Gaussian approximation of the point target response in the BH model. The estimated P_u is converted in dB and corrected by atmospheric correction and scaling factor, whose fields are contained in the mission data. This constitutes the σ_0 output of the algorithm (backscatter coefficient). The epoch is not provided in the output since its precision and accuracy has not been verified.

The "Fitting Error on the leading edge" (Err) is used as a quality measure for the fitting. It is computed as the RMS difference between the fitted and the real waveform, considering only the gates of the leading edge. When Err>0.3, the quality flag is set to 1, i.e. the quality of the fitting is bad.

Once the full SGDR has been retracked, a further step can be applied to remove the "intra-1Hz correlation" between τ and SWH. WHALES will be applied in the Round Robin with and without this additional step.

2.1.4 Definitions

BROWN-HAYNE MODEL

WHALES is based on the Brown-Hayne (BH) functional form that models the radar returns from the ocean to the satellite. The BH theoretical ocean model [Brown (1977), Hayne (1980)] is the standard model for the open ocean retrackers and describes the average return power of a rough scattering surface (i.e. what we simply call waveform). The return power is modelled as follows (equations as reported in Passaro et al., 2014):

$$V_m = a_\xi P_u \frac{[1+erf(u)]}{2} exp(-v) + T_n$$

where:

$$a_\xi = exp(\frac{-4sin^2\xi}{\gamma}); \qquad \gamma = sin^2(\theta_0)\frac{1}{2ln(2)};$$

$$u = \frac{t-\tau-c_\xi\sigma_c^2}{\sqrt{2}\sigma_c}; \qquad v = c_\xi(t - \tau - 0.5c_\xi\sigma_c^2);$$

$$\sigma_c^2 = \sigma_p^2 + \sigma_s^2; \quad \sigma_s = \frac{SWH}{2c};$$

$$c_\xi = b_\xi a; \qquad a = 4c / [\gamma h(1 + \frac{h}{R_e})];$$

$$b_\xi = cos(2\xi) - \frac{sin^2(2\xi)}{\gamma}$$

where $erf(u)$ denotes the error function, c is the speed of light, h the satellite altitude, R_e the Earth radius, ξ the off-nadir mispointing angle, θ_0 the antenna beam width, τ the Epoch with respect to the nominal tracking reference point, σ_c the rise time of the leading edge (depending on a term σ_s linked to SWH and on the width of the radar point target response σ_p), P_u the amplitude of the signal and T_n the thermal noise level.

NELDER MEAD ALGORITHM

The Nelder–Mead (NM) algorithm is a simplex optimisation method that does not use the derivatives of its cost function, whilst it searches for the minimum in a many-dimensional space. Specifically, considering m parameters to be estimated, given that a simplex of dimension m is a polytope of the same dimension and with m + 1 vertices characterised by m + 1 cost function values,NM generates at each step a new point whose cost function is compared with its value at the vertices. If it is smaller, the point becomes a vertex of the new simplex and a new iteration is generated (Nelder and Mead, 1965). Convergence is reached when the diameter of the simplex is smaller than a specified tolerance.

In WHALES, the objective function to be minimised is:

$$C = \sum \left[W * R^2 \right]$$

where W is the vector of weights and the residual R is the difference between the real and the fitted waveform. NM is applied using the Python package scipy.optimize.minimize.

WHALES COEFFICIENTS

The key concept of the WHALES subwaveform is that a leading-edge only retracker, although also providing results waveforms that do not conform to the BH model, has worse noise performances than a full-waveform retracker and therefore would not guarantee the homogeneity of the result. For best accuracy the subwaveform width for the second pass must be optimised such that it fully includes all gates comprising the leading edge, but with minimal contribution from the trailing edge, where artefacts such as bright target responses may prevent the BH model from accurately describing the shape. Defining startgate and stopgate the first and last gate of the subwaveform of choice, in effect the issue is one of defining an appropriate stopgate for a given SWH. The relationship between SWH and stopgate was derived from Montecarlo simulations. For each value of SWH ranging from 0.5 to 10 m in steps of 0.5 m, 10000 echoes were simulated with the BH model adding realistic Rayleigh noise, and then averaged to create a simulated high-rate waveform. The resulting waveforms were retracked over the entire waveform, and then over sub-waveform windows with startgate=1 and variable stopgate, and the RMS errors (RMSE) were computed.

The difference of the RMSEs between the "full waveform" estimate and the subwaveform estimates is displayed as a function of the stopgate position in the figure below (upper panel). The x axis is, in practice, the width of the sub-waveform, expressed as number of gates from the tracking point to the stopgate. The results for each SWH level are coded in different colours. For all three parameters, the curves converge asymptotically to the full waveform estimates, as expected for this idealised case of "pure-Brown" response of the ocean surface. The relation needed for step XXX of WHALES is shown in the panel below and is obtained by setting a tolerance in the RMSE difference of the SWH. In order for WHALES to optimise the need to retrieve signals whose trailing edge is corrupted, the tolerance bar was set to 2 cm at 20 Hz, i.e. 0.45 cm at 1 Hz.
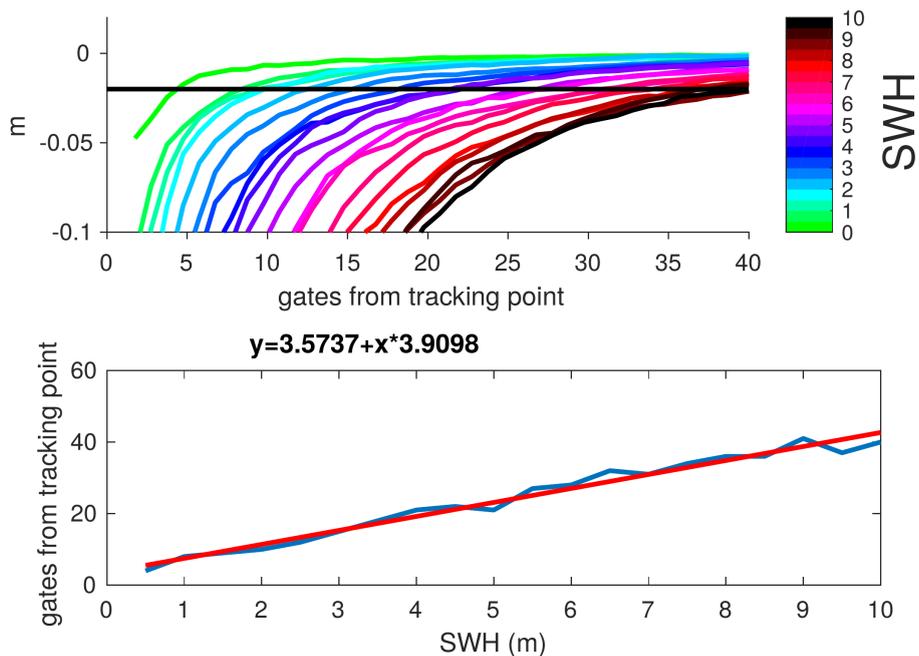
Figure 2: (Up) Difference of the RMSEs between the "full waveform" estimate and the subwaveform estimates as a function of the stopgate position. (Below): linear relationship obtained by setting a tolerance in the RMSE difference of the SWH in the upper plot. In order for WHALES to optimise the need to retrieve signals whose trailing edge is corrupted, the tolerance bar was set to 2 cm at 20 Hz.

WEIGHTS

To derive the adaptive set of weights that is used to find convergence in WHALES, a Monte Carlo simulation is performed. The objective is to base the weighting on the uncertainty of the fitting along the leading edge of the waveform. As an estimation of the uncertainty, the standard deviation (STD) between the simulated echo and a large number of fitted waveforms is used.

Simulated echoes are generated according to the BH model as previously reported, SWH at steps of 0.5 m from 0 to 10 m (10000 waveforms per SWH value). Each echo is retracked with a BH retracker that finds the convergence through an unweighted Nelder-Mead. For each SWH value:
- the value of the residuals between the simulated echo and the fitted waveform is stored
- the position of the start and the end of the leading edge is stored
For each SWH value, there will be 10000 value of residuals at each waveform gate, and we can therefore compute their std. The weights to be used in the WHALES retracking will be the inverse of this std, i.e. the so-called "Statistical Weighting", which in statistics is a

recommended choice when the uncertainties of the different points to fit are very different from each other (Wolberg, 2006).
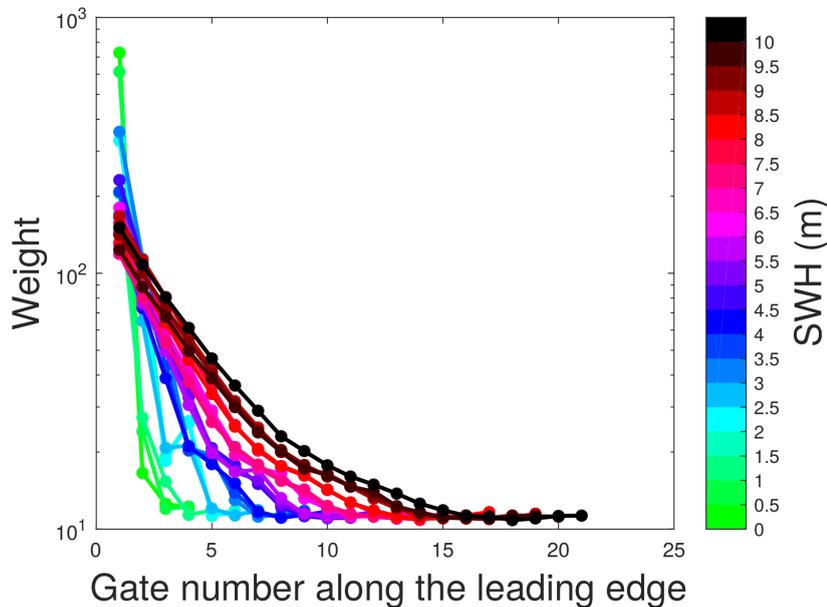

Figure 3: Variable weights used by WHALES depending on Significant Wave Height and gate number along the leading edge of the waveform.

INSTRUMENTAL CORRECTION FOR WHALES

2.1.5 Function

Most retracking algorithms that assume a mathematical form for the pulse shape model it as a Gaussian. This is clearly incorrect as a Gaussian curve is theoretically of infinite extent, but is convenient because then the convolution of the pulse with the height p.d.f. of reflecting facets remains a mathematically tractable form, a Gaussian too, The actual shape of the emitted pulse, recorded as the Point Target Response (PTR) can also be modelled as a sinc function (F. Boy, pers. comm.) The algorithm detailed here provides a correction to the WHALES estimation to compensate for the simplifying assumption of Gaussian pulses. The effect only has significant variability at low wave heights (narrow p.d.f. of height of reflecting facets), but also changes depending on how the sampling bins align with the return echo i.e. the sub-gate positioning of the waveform leading edge.

2.1.6 Algorithm Definition

INPUT:
- Look-up Table (LUT) of correction
- SWH & epoch estimates from WHALES

OUTPUT:
- Corrected SWH

2.1.7 Algorithm Background

Simulations were performed to generate waveforms using either the real PTR shape or the Gaussian approximation, and then both sets retracked by WHALES. The difference is then tabulated as a function of SWH and waveform position.

The LUT will be discretized at steps of 0.10m in SWH and 1/16 gate in tk_point (position of leading edge), with the relevant indices being defined as:
    i = floor(SWH/0.1);
    j = 16 * (tk_point - floor(tk_point))
with both indices starting from zero. This LUT is illustrated in Figure 4
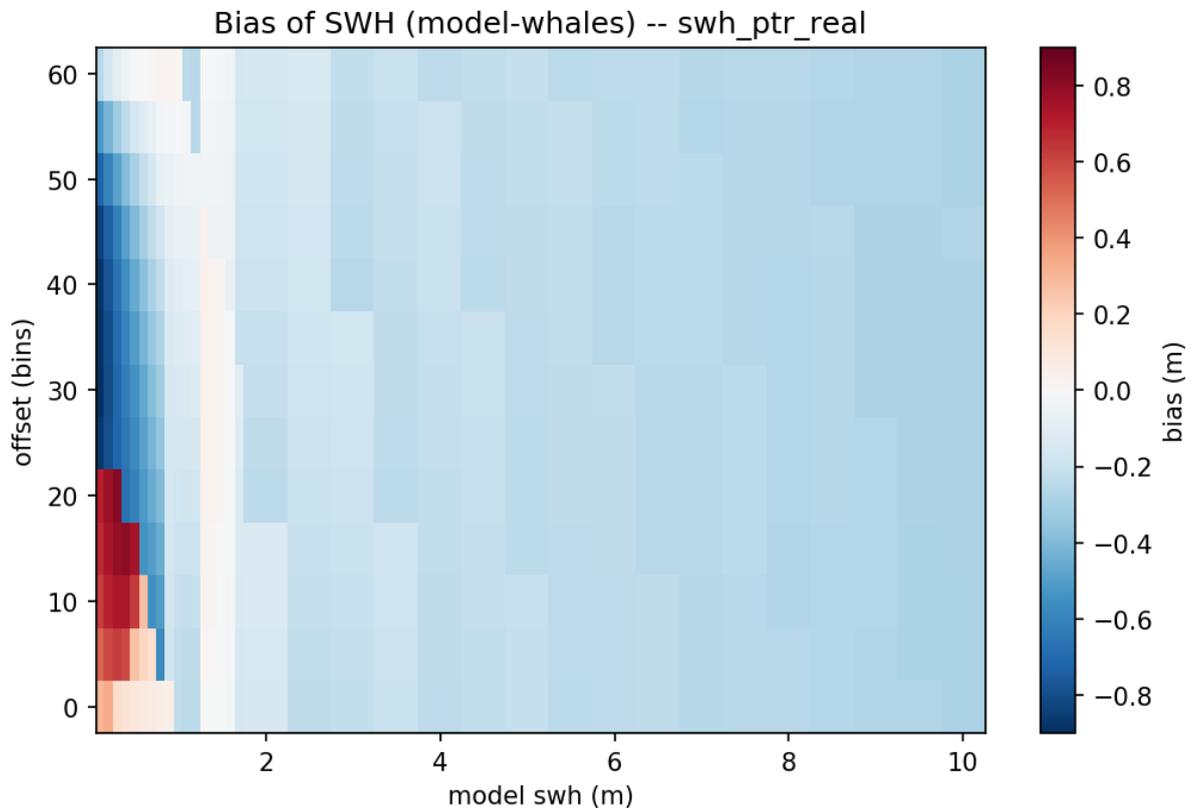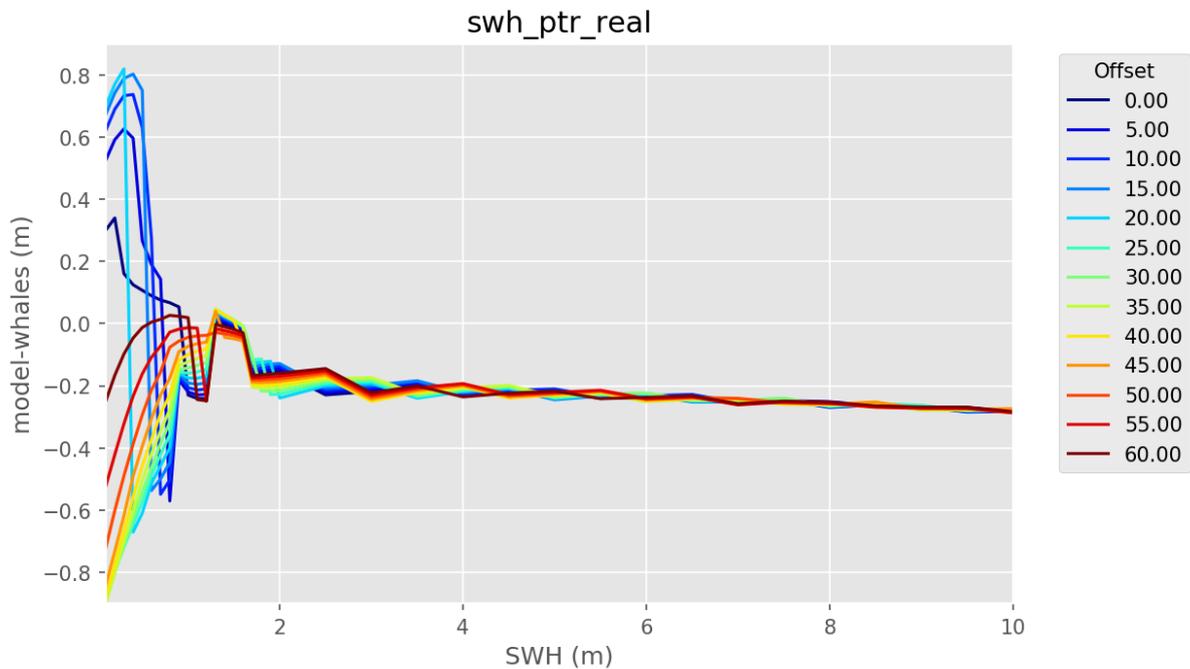
Figure 4 : Correction to be added to SWH_orig_WHALES as a function of that value and of the position of the leading edge; here we use bin as a fraction (1/64) of a waveform gate. The same data are shown in the upper and lower plots; the different pictorial representations are to provide greater understanding of how sharp the changes are. Note for SWH>2m the correction is small, slowly-varying and not affected significantly by the position of the leading edge. Knowledge of the position of the leading edge is only important for wave heights less than 1.0m.

As part of the evaluation of the simulation code, a similar exercise was carried out using the MLE3 retracker, and noting the PTR correction we derive, and comparing with that tabulated in the Jason-3 SGDRs. Figure 5 shows that according to our simulations, the MLE3 retracker should also have a PTR correction that depends upon the position of the leading edge within the sampling. The official tabulated correction does not correspond to the mean over all eventualities, but matches closely to one particular position of the leading edge (in our nomenclature a shift of 5/64 of a gate). It is likely that an improved PTR correction for MLE3 (and MLE4) retracker could be implemented, if the agencies were particularly interested in these low wave height conditions.

Bias of SWH (model-mle3) -- swh_ptr_real

swh_ptr_real
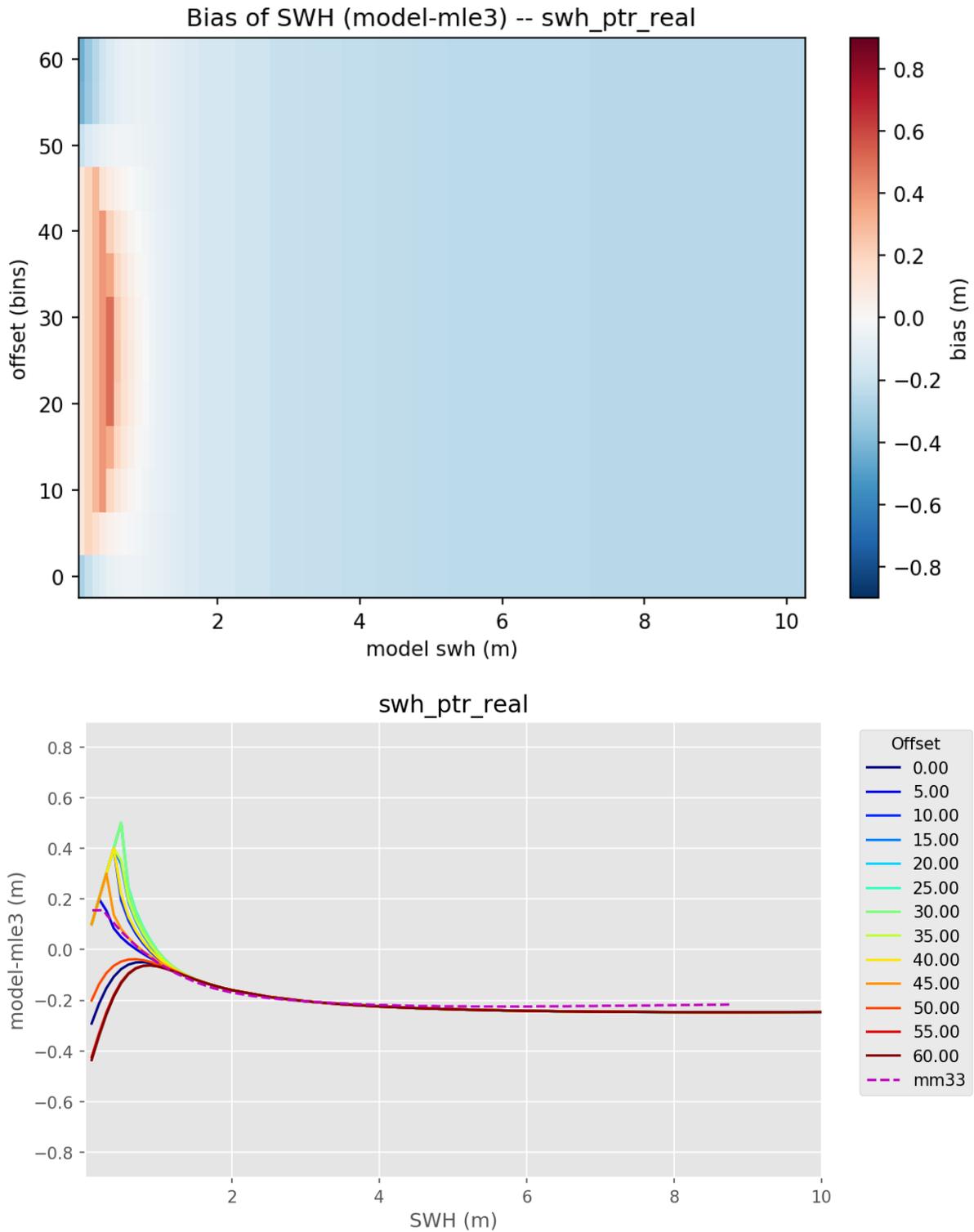
Figure 5 : Our derived PTR correction to be added to SWH_orig_MLE3 as a function of that value and of the position of the leading edge. Note again great variability with waveform position offset for wave heights less than 1.0m. The relationship routinely implemented in the Jason-3 SGDRs (denoted mm33 here, and shown by purple dashed line) does not correspond to the mean over all possible offsets, but matches well with one particular position of the waveform.

INTRA-1Hz CORRECTION FOR WHALES

2.1.8 Function

Any particular realization of fading noise affects the signal in individual waveform bins, and causes errors in the retrieval of the shape parameters (amplitude, position of leading edge and its slope, ...). Depending upon the retracker algorithm used, there may be covariance between these noise-induced errors, and therefore information about the likely error in one term can be used to infer an adjustment to the estimate of another term (Quartly et al., 2019; Quartly, 2019). For the specific case here, an adjustment to SWH can be found from the anomaly in range relative to the local average.

2.1.9 Algorithm Definition

INPUT:
- Time series of time, range, altitude and corrected SWH, all at 20 Hz
- Small file of coefficients to be applied

OUTPUT:
- Adjusted SWH

2.1.10 Algorithm Background

The correction is applied to the composite pulse width (sigmaC) and is related to the anomaly in (altitude minus range). Regression coefficients were calculated between anomalies in SWH and in altitude minus range, (a_r) as detailed in Quartly et al.(2019). [Note, some algorithm developers adopt the convention of returning negative values for SWH if the square was negative; this code allows for that in its conversions between $_c$ and SWH;. If developers simply set SWH to zero when the derived square is negative, information is lost, but this code accommodates that.]

a_r_{21} = 21-point moving mean of a_r (assuming that at least 11 of the supplied points have valid SWH and valid a_r)

σ_C = sqrt (2.57 + SWH. |SWH| / 0.36)

σ_{C2} = σ_C+ γ(a_r - a_r_{21})

SWH2 = (σ_{C2}^2 - 2.57) * 0.36

SWH_{adj} = sqrt(|SWH2|).sign(SWH2)

2.2 ATBD-2: ADAPTIVE NUMERICAL RETRACKER (CLS)

2.2.1 Function

To perform the numerical retracking (hereafter called "adaptive" retracking) on the waveforms (main band), i.e. to estimate the altimetric parameters (epoch, composite Sigma, amplitude, "mean square slope").

This retracker is designed to provide optimal heights over all surface types. It can thus be activated over different surfaces with different backscattering properties.

2.2.2 Algorithm Definition

INPUT:

- Waveform:
    - Waveform
    - Waveform validity flag
    - Waveform classification from neural network approach as described in Poisson et al., [2018]
- Orbit:
    - Orbit altitude (20-Hz)
- Altimeter instrumental characterization data:
    - Altimeter instrumental characterization data for the preparation of data for the ocean retracking (Point Target Response and Low Pass Filter)
    - Abscissa of the reference sample for tracking
    - Sampling interval of the analysis window
    - Antenna beamwidth
    - Ratio between the PTR width and the sampling interval of the analysis window
- Universal constants (SAD):
    - Light velocity
    - Earth radius

OUTPUT:
- Epoch: t
- Composite Sigma: s_c
- Amplitude: P_u
- Gamma parameter:
- Thermal noise level: P_n
- Number of iterations
- Mean Quadratic Error
- Quality information, such as an execution flag (valid / invalid)

MATHEMATICAL STATEMENT:

Background

The aim of the adaptive retracker algorithm is to make the measured waveform coincide with the return power model, according to a Nelder-Mead simplex method. This fitting method has the advantage to consider the exact likelihood criterion compared to Newton-Raphson and so, to fully account for the speckle noise statistics. It is known to be one of the most effective methods for the minimization of estimation errors. Besides, the adaptive retracker uses a numerical approach allowing the introduction of the real PTR in the echo model instead of a Gaussian approximation (improving the quality of the model and removing the need for Look Up Table Corrections).

The adaptive retracking algorithm is performed on the Ku-band waveforms only.

Model computation

The adaptive retracker is based on a model directly derived from the Brown Model (Brown, [1977]). But unlike traditional ocean models, this model accounts for the mean square slope of the surface, giving to the adaptive retracker the ability to be used over surfaces of different roughness (diffuse or peaky echoes). To do so, the dependence of the sigma naught to the incidence angle is no longer ignored, using the formulation proposed by Amarouche et al. [2010]:

$$\sigma_0(\theta) = \sigma_0(0)\exp(\frac{-\sin^2(\theta)}{mss})$$

with Θ being the incidence angle and mss the mean-square surface slope.

Initially, this model, similar to the Hayne model, is a composite signal corresponding to the convolution of three terms: the flat sea surface response to a Dirac radar pulse, the impulse response (altimeter response to a point target), and the wave distribution (the distribution of heights of surface points). In numerical retracking, the return power model corresponds only to the sea response to a Dirac radar pulse (with no impulse response, as we introduce the real PTR by convolution). The expression of the return power as a function of time is given by:

$$S(t) = \frac{A\,\sigma_0}{2}\left\{\left[1 + erf\left(\frac{t - \tau - \frac{4c}{\Gamma h}\sigma_c^2}{\sqrt{2}\,\sigma_c}\right)\right]\exp\left[-\frac{4c}{\Gamma h}\left(t - \tau - \frac{2c}{\Gamma h}\sigma_c^2\right)\right]\right\} + N_t$$

(1)

with:

- o σ_0 the ocean surface backscattering cross-section at normal incidence
- o $\sigma_c^2 = \frac{SWH^2}{4c^2}$; $SWH = 2c\sigma_c$ (significant waveheight)
- o t : round-trip time delay (equivalent to the distance satellite/sea surface),
- o tau : delay time of the radar pulse return from the mean sea surface so called epoch
- o c = velocity of light, h = mean (raw) satellite altitude

○ N_t is the thermal noise level

$$\Gamma = \frac{4\gamma mss}{4mss + \gamma}$$

○

$$\gamma = \frac{2}{Log_e(2)} \cdot \sin^2(\frac{\theta_0}{2}), \text{ with } \theta_0 \text{ the antenna beamwidth}$$

Optimization principle

Based on this formulation, the Adaptive algorithm aims at estimating the following parameters:

- tau   : the epoch
- $sigma_c$: the composite Sigma
- P_u : the amplitude
- Gamma   : the Gamma Parameter (and the shape parameter *mss* derived from it)

The optimization is based on the iterative Nelder-Mead simplex method that uses the exact maximum likelihood criterion with no approximation or derivatives of it. In this respect, it provides unbiased estimates contrary to least square estimators.

The principle of the Nelder-Mead method consists in reshaping a simplex for minimizing the objective function, manifested by expansions or successive contractions of the simplex according to the local topology. A schematic view of the principle is given in the figure 6 below.

(a) Reflection if $f(X_r) < f(X_1)$
and $f(X_r) \leq f(X_e)$ or if
$f(X_1) \leq f(X_r) < f(X_n)$

(b) Expansion if
$f(X_e) < f(X_r) < f(X_1)$

(c) Outside contraction if
$f(X_n) \leq f(X_r) < f(X_{n+1})$
and $f(X_c) < f(X_r)$

(d) Inside contraction if
$f(X_{n+1}) \leq f(X_r)$
and $f(X_{cc}) < f(X_r)$

(e) Shrinkage in
other cases
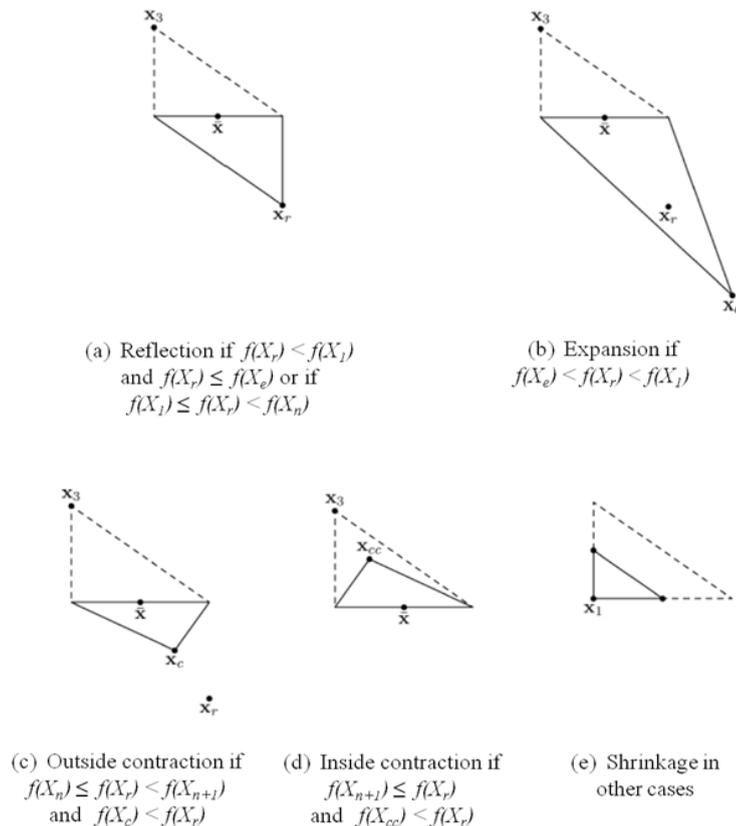
Figure 6: Illustration of the Nelder-Mead optimization method.

As previously mentioned, this method uses the exact maximum likelihood criterion for the convergence (and not the partial derivatives of the likelihood) which makes it more robust than the classic methods to achieve convergence even though it requires higher number of iterations (also lowering the processing time). The maximum likelihood criterion accounts for the exact noise statistic (considering the number of decorrelated pulses) whereas classical approaches do not.

In this case the maximum likelihood is expressed as following:

$$C = Cste + Ndec \sum_{1}^{n} \frac{signal(n)}{mod(n)} + (Ndec - 1) \sum_{1}^{n} \ln(signal(n)) + (Ndec) \sum_{1}^{n} \ln(mod(n))$$

With:

signal(n) = nth sample of the observed signal
mod(n) = nth sample of the modeled signal
Ndec is the number of decorrelated pulses

The main steps of the processing are the following:

- Identification of the waveform validity:
    - The validity of the waveform is determined from the input waveform quality information. The retracking is then performed only if the input waveform is valid.
- Thermal noise estimation:
    - The thermal noise level (Nt) is computed from an arithmetic average of samples of the first plateau (in a range of gates defined as processing parameters).
- Initialization:

- When available, we use the MLE4 estimates to initialize the epoch, the composite sigma and the amplitude. Default values of the epoch, composite sigma and amplitude (processing parameter) are used otherwise.
- Minimization of the cost function is performed by the Nelder-Mead method
  - This iterative estimation process is stopped when the convergence criteria is reached.
- Set the quality flag
  - The mean quadratic error (MQE) between the normalized waveform and the corresponding model built from the estimates is computed. The estimates with a MQE below a certain value are valid and must be kept. The others are considered non-valid and have to be edited. Based on this criterion, a quality flag provided at 20 Hz is set at "0" when the estimate is valid, otherwise is set at "1" (0=good;1=bad). This quality flag is to be used for the data analysis at 20Hz and to compress them at 1Hz.

Comments

The radar backscattering model remains valid at any satellite altitude as long as the sea-surface area illuminated by the -3dB antenna beamwidth is larger than the effective footprint defined by the receiving window width.

Also note that the waveform samples are in counts and not in watt power units, in order to avoid any issues in processing very high and low values (corresponding respectively to very high and low values of the backscattering coefficient of the sea surface).

INTRA-1Hz CORRECTION FOR ADAPTIVE RETRACKER:

2.2.3 Function

To compute 20-Hz corrected Ku-band ocean significant waveheight for correlated high-frequency errors.

2.2.4 Algorithm Definition

INPUT DATA

- 20-Hz Ku-band ocean significant waveheight
- 20-Hz Ku-band ocean range
- validity flag

OUTPUT DATA

- 20-Hz corrected Ku-band ocean significant waveheight

MATHEMATICAL STATEMENT

An empirical high-frequency correction based on range noise is applied on nominal 20-Hz SWH. The approach is similar to the one defined by Zaron and DeCarvalho [2016] to correct sea surface height estimations.

3. Algorithms for Satellite Altimetry (Delay Doppler Mode) Processing

3.1 ATBD-3: WHALES for SAR

3.1.1 Function:

The aim of this algorithm is to provide significant wave heights (SWH) from SAR altimetry waveforms both in the open ocean and the coastal zone. For each high frequency observation a SWH and backscatter coefficient σ_0 is provided as well as a quality flag each.

The same algorithm for Open Ocean and coastal zone is used to ensure consistency and continuity of the SWH observations.

3.1.2 Algorithm Definition:

Input Data:

- Sentinel-3A L1b products with SAR waveform
- Look-Up table for point target response

Output Data:

- Significant wave height (SWH)
- Quality flag for SWH. 0 for usable values, 1 for corrupted.
- Backscatter coefficient σ_0.

Mathematical Statement:

The rising time of the leading edge is related to the significant wave height (SWH) of the reflective surface. Thus, we develop a subwaveform retracker which only considers the part of the SAR waveform around the leading edge. From the ALES+ retracker (Passaro et al. 2018), the retracker inherits the subwaveform detection and the fitted function. The relationship between the rising time of the leading edge and SWH is determined in a Monte-Carlo simulation environment.

Subwaveform retracker:

The procedure is summarized in Fig 1. After the subwaveform extraction two runs of function fitting are performed which lead to the final estimation of the parameters SWH, σ_0, and their quality flags.
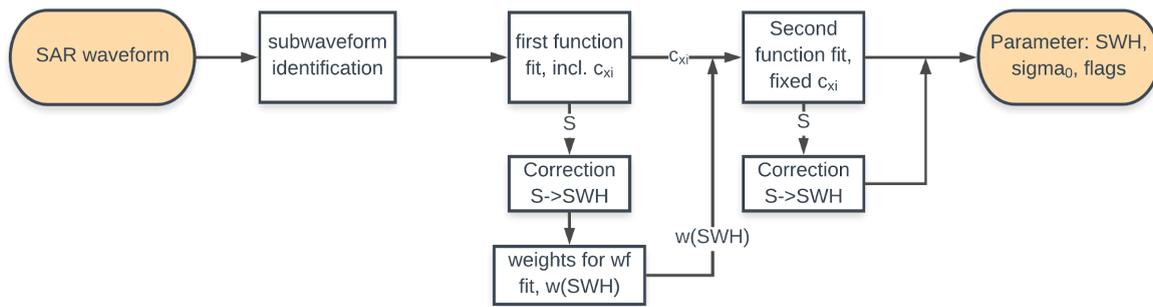
Figure 7: Flow diagram of WHALES for SAR

In order to extract the subwaveform from the whole SAR waveform the following steps are executed:

1. Normalisation of the waveform by its maximum power
2. The end of the subwaveform is defined as 10 gates after the gate where the waveform reaches its maximum power. The number of 10 gates have been found empirically to be accommodating different waveforms with different trailing edge slopes.
3. The start of the subwaveform is search backwards from the maximum power gate where for the first time the difference between consecutive gates is smaller than 0.01. We found this threshold value satisfied our aim finding the beginning of the leading edge without including too much of the thermal noise.

The functional form fitted to the subwave form is the Brown-Haynes model, which was originally developed for LRM altimetry waveforms.

The fit is performed twice: In the first run all bins of the subwaveform are weighted equally. The fitting returns the estimated parameters т (position of leading edge), S (rising time of leading edge), and A (amplitude). In this run an additional parameter is estimated, the slope of the trailing edge c_xi. From this first run the rising time of the leading edge S is extracted from which a first estimate of the SWH can be gained with the analytical function found in the Monte-Carlo-Simulation (see detailed description below).

In the second run of the fitting procedure the slope of the trailing edge c_xi is fixed to the estimated value of the first round. In this run not all bins are weighted equally but weights are chosen based on the preliminary SWH of the first run. These weights were again found empirically with the Monte-Carlo-Simulation (see detailed description below).

The fit is done with the numerical Nelder-Mead algorithm which is included in many premade optimization packages, e.g for Python in scipy.optimization.minimize. For both fitting runs the algorithm requires initial values. т_0: mean position between start of subwaveform and maximum; S_0: rising time between the start and maximum of subwaveform; A_0: two times the mean of the subwaveform. See Figure 8 for an example of the first and second fit of an Sentinel-3 SAR waveform.
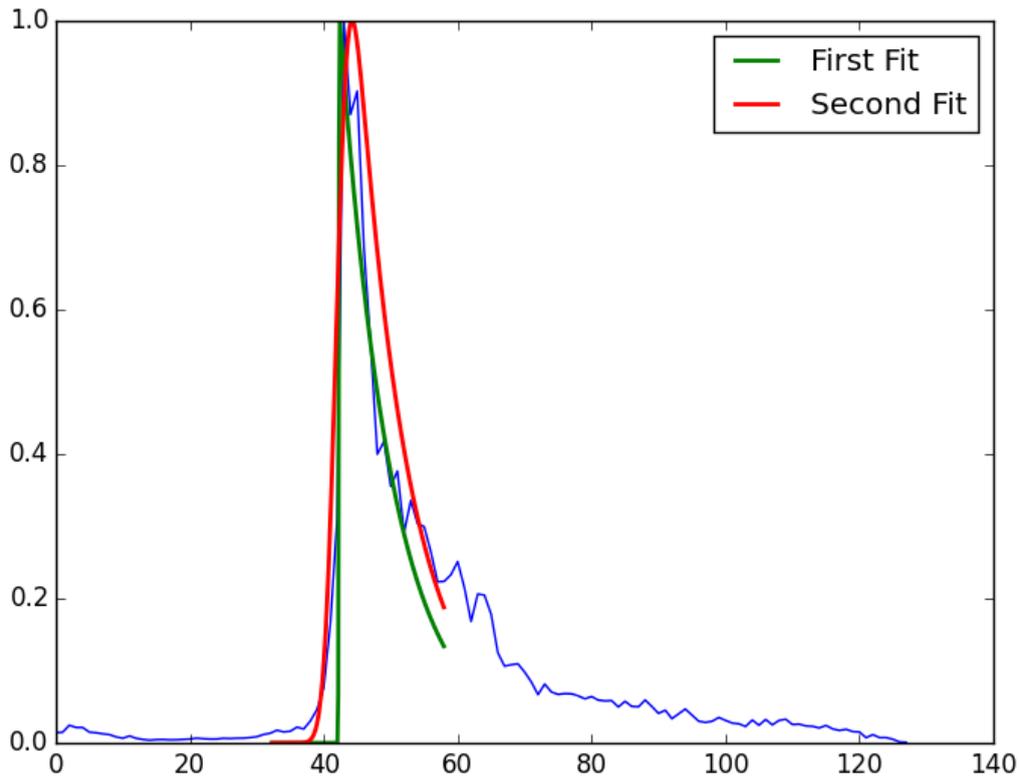
Figure 8: Fitting of real Sentinel-3A waveforms

From the second function fit again the rising time of the leading edge S is extracted and converted to SWH. The algorithm provides also an estimation of the backscatter coefficient σ_0 with $\sigma_0 = 10 * log_{10}(A * normalizefactor)$ (the normalize factor was used in the subwaveform identification above).

For the parameter SWH a quality flag if they are usable or not is provided. The flag is based on the fitting error (root mean square of the residuals) of the second function fit. If this error is larger than 10% of the maximum power the flag is set to 1, i.e. the SWH value should not be used.

Monte-Carlo-Simulation:
Correction S to SWH:
In order to establish the relationship between rising time of the leading edge S and SWH we implement a SAR multilook-waveform simulation following the formula of Gommenginger et al. (2017). In the simulation the point target response (PTR) is dependent from SWH and used according to the look-up table provided in Gommenginger et al. (2017). With the waveform simulator a Monte-Carlo-Simulation can be established with changing SWH, waveform amplitude, central gate epoch, and antenna mispointing angle in track and across track direction. For each waveform at each bin a normal distributed random noise with a standard deviation of 1% of the waveforms amplitude is added. Thus, the standard deviation of the noise is constant for all bins of one waveform.

Each simulated waveform is retracked with our subwaveform retracker and the rising time of the leading edge is extracted. From this we found the analytical relationship between the rising time *S* and SWH:

$$SWH = \sqrt{28.6 \cdot S + 29.5} - 8.2$$

Weighting factor:

With the same Monte-Carlo-Simulation the weights for the second fitting round are estimated. To this end, for different SWH (0-15m, 0.5m steps) 4000 simulated waveforms are investigated. For each simulated waveform the Brown-Haynes model is fitted to the subwaveform (see above) and the residuals for each bin of the subwaveform are stored.

Afterwards, for each SHW value the residual r^j_i are collected for each bin i (starting with the first bin of the subwaveform) in the jth simulated and fitted waveform. The weight for the ith bin of the subwaveform with an estimated SWH is then:

$$w(i,\ SWH)\ =\ 1/std(r^j_i)$$

The weights outside the subwaveforms are zeroes, i.e. only the subwaveform is fitted.

3.2 ATBD-4: L1A to L1B-S/L1B processing chain

The role of isardSAT within the Sea State CCI project is to optimise the Delay-Doppler (DD) or SAR mode processing chain starting from L1A Sentinel-3 products in order to provide improvements in the retrieval of the significant wave height (SWH). The core of the Delay-Doppler processor is based on DeDop platform (https://DeDop.org/) that offers high versatility on the setting of the processing options ingesting L1A Sentinel-3 input data (Cotton et. al 2018).
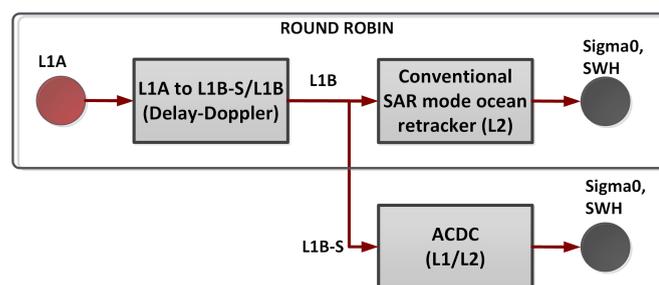
Figure 9: isardSAT processing framework within the Sea State CCI project: only the L1A to conventional L1B/L2 processing will be considered in the round robin.

The exploitation of the outcomes of the Delay-Doppler processor within the Sea State CCI is schematically sketched in Figure 9. On one side, the conventional[1] L1B product will be

---

[1] From now on we refer to conventional processing or L1B products when considering the normal Delay-Doppler processing without any application of the ACDC processing stage and so the related L1B products with the ocean retracking stage. This processing branch from L1A to L2 will be considered on the round robin exercise.

exploited by the in-house isardSAT SAR mode ocean retracker (Makhoul et al. 2018) and based on the SAR ocean model developed by Ray *et. al* 2015a. Different processing options (or algorithms) can be configured and tested in order to optimize the performance of the geophysical retrievals exploiting the conventional L1B product in the conventional SAR mode

On the other side, the promising algorithm amplitude compensation and dilation compensation (ACDC), initially developed at burst level and developed by Ray et. al. 2015b, will be adapted to operate at stack level (*Makhoul et. al. 2018*). Therefore, the ACDC algorithm is exploiting the intermediate L1B-S product (stack product[2]) to generate an equivalent ACDC waveform (L1B) and the related geophysical parameters (like SWH). ACDC processing allows to implement a simpler and faster retracker, which is intrinsically included in the processing itself as specific initial estimates of epoch and SWH are required for its operation. Hence, ACDC can be understood as a L1+L2 processing.

NOTE: The ACDC algorithm is not going to be exploited within the altimetric round robin exercise. It has been included for completeness, as it is part of isardSAT research activities within the Sea State CCI project. Initial analysis with CryoSat-2 data have shown very good performances in terms of noise compared to the conventional L1B processing (Makhoul et al. 2018). Hence, the outcome of the analysis of the ACDC over Sentinel-3, within the Sea State CCI, may open new options on the way the L1A to L1B processing shall be considered.

The aim of this subsection is to describe the L1A to L1B-S/L1B processing, which is the starting point for the subsequent algorithms. The SAR ocean waveform retracker for the conventional SAR waveforms is described in subsection 3.3 (L2 processing), and the ACDC algorithm in section 3.4 (L1+L2 processing).

3.2.1 Function:

The aim of this algorithm is to produce conventional SAR multilooked power waveforms equivalent to the L1B waveforms of the operational Sentinel-3 L1A to L1B processor. At the same time will produce L1B-S stack products to be exploited by the ACDC.

The Delay-Doppler altimeter uses the power backscattered from the scene more efficiently than does the classical altimeter, since the whole beam-limited along-track signal is exploited, instead of the pulse-limited area typically considered by classical altimeters, as schematically sketched in Figure 10. This is achieved thanks to the proper slant range (or delay) variation compensation. The extra delay observed from each Doppler bin in which the along-track beam is partitioned is removed, aligning all the Doppler beams to the same delay or range, known as range migration correction (RMC, see figure 10).

---

[2] In Delay-Doppler processing, the stack is an intermediate product that contains the different waveforms from different bursts that have been focused to a specific surface location (analogous to the so called Delay-Doppler map). An incoherent averaging of them produces the final conventional multilook DD or SAR waveform.
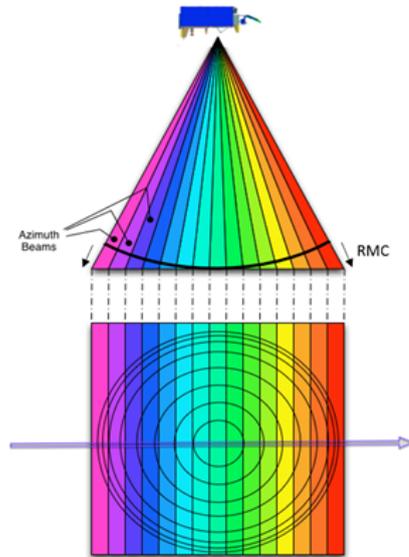
Figure 10: Delay-Doppler altimeter's illumination geometry side (top) and footprint (bottom) plan views. The along-track beam is partitioned in several Doppler beams with improved resolution. An extra delay or range per beam needs to be compensated, by introducing the range migration correction-RMC (credit: ESA).

The block diagram of the L1A to L1B processor is sketched in Figure 11. The main processing algorithms are:

- Instrument/processing gain corrections
- Waveforms corrections
- Surface locations
- Beam angles computation
- Azimuth processing (beam-forming)
- Stacking
- Geometry corrections
- Range compression
- Stack masking
- Multi-looking
- Sigma0 scaling factor
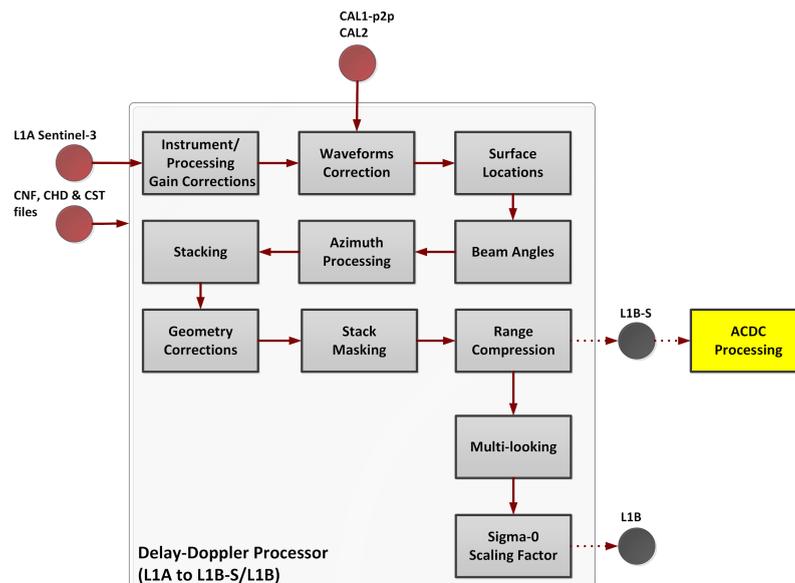
Figure 11: Block diagram of the Delay-Doppler or SAR processor from Sentinel-3 L1A to L1B-S/L1B based on DeDop chain; ACDC processing to be considered as a plug-in to DeDop, exploiting the L1B-S product; CNF, CHD and CST stand for configuration, characterization and constants' file; (credit: isardSAT).

3.2.2 Algorithm Definition:

Input Data:

- Sentinel-3A L1A products
- Configuration file
- Characterisation file
- Constants file

Output Data:

- Equivalent Sentinel-3 L1B-S/L1B products.

Instrument/processing gain corrections: to obtain a meaningful estimation of the received power at the flange of the antenna, the input waveforms shall be properly calibrated in terms of power, accounting for instrumental as well as specific processing gains.

Waveforms corrections: applied to the different samples of the different pulses within each burst to account for intra-burst amplitude/phase variations (CAL1-p2p) and amplitude deviations due to the low-pass filter (CAL2) modulation as indicated in Dumont2016.

Surface locations: in charge of computing the on-ground positions where the L1B measurements will be sampled at.

<u>Beam angles computation</u>: the angles between the satellite velocity vector and the vector connecting every surface location at each satellite's burst location are determined (required for beamforming operation).

<u>Azimuth processing (beam-forming)</u>: this step generates and points the fine Doppler beams towards the computed on-ground surface locations. Specific intra-burst weighting can be also applied to reduce the impact of the side-lobes of the Doppler beams in the range-Doppler map.

<u>Stacking</u>: groups the beams from the different bursts pointed to each one of the sample locations, generating the so called stack map.

<u>Geometry corrections</u>: for each surface location and due to the different observing geometry, each beam of the stack needs to be aligned in range to concentrate the energy around a reference range, such that the incoherent averaging can be effectively performed.

<u>Range compression</u>: this stage is in charge of transforming the input stack from time-domain to frequency-domain, which encodes the range information via an FFT. Afterward the power waveforms are generated taking their intensities.

<u>Stack masking</u>: this algorithm filters out specific samples of the stack that may impair the L1B waveforms, as wrapping of the samples due to geometry corrections, land contamination (Garcia-Mondéjar2016), Doppler ambiguities as in Sentinel-6 (Roca2016). At this point the stack information can be extracted and included in the so called L1B-S product to be exploited later on by the ACDC processing.

<u>Multi-looking</u>: an incoherent averaging of the beams within the stack is carried out. The samples that have been artificially set to zero during geometric corrections or stack masking can be either included or discarded in the multi-looking process. This multilooking only applies to obtain the conventional L1B SAR mode waveform.

<u>Sigma-0 Scaling factor</u>: translates the received power at the flange of the antenna into radar backscattering coefficients sigma0.

An additional processing module incorporated in the L1B and that can be optionally activated is the promising ACDC. It is based on the original approach proposed by Ray et. al. 2015b, but in this case operates directly over the Delay-Doppler stacks; providing the geophysical parameters (sea-surface height, significant wave-height and sigma0) directly at L1B, since in this case the retracker is an integral part of the ACDC processor. This is different from the conventional L1B processing (doesn't include ACDC), where the geophysical parameters are extracted at L2 with a given conventional retracker.

isardSAT roles in the CCI sea state project is to find the optimized processing baseline at L1B to improve the retrieval of the SWH. The different processing options that can be tested in order to find the optimized L1B conventional processing (with no ACDC) are:
- <u>Burst azimuth weighting</u>: Specific windowing can be optionally applied within the burst to reduce the impact of the along-track side-lobes in the final stack

- Azimuth processing method: exact or approximate; areas with high topographic variability might be processed using the more computationally demanding exact method, while smooth scenarios can be efficiently processed with the approximate one.
- Antenna weighting: compensate the effect of the antenna pattern modulation at stack level prior to multi-look processing
- Multi-looking with zeroes method: zero-valued samples (forced by the masking process) can be included or not in the incoherent processing
- Zero-padding in across-track (range oversampling factor): decreasing the range bin spacing offers a better sampling of the waveforms (potentially improving re-tracking for very specular returns with low SWH)

3.3 ATBD-5: Conventional SAR mode ocean retracker

3.3.1 Function:

The aim of this algorithm is to invert specific geophysical parameters (like SWH, sigma0 and SSH) from the altimeter measurements, based on fitting a theoretical model of the SAR ocean backscattered signal to the L1B altimetric waveforms.

The in-house isardSAT SAR mode or Delay-Doppler ocean retracker is based on the original model derived by Ray et al. 2015, proposing the first closed-form expression for the SAR altimeter ocean backscattered echo. A block diagram of the L2 processor incorporating such retracker is depicted in Figure 12.

The main processing blocks are:
- pre-processing:
- waveform modeling:
- fitting procedure:
- geophysical corrections: are applied to remove any environmental-dependent effects on the altimeter measurements[3].

---

[3] Geophysical corrections impairing the measured range are applied to the estimated sea surface height; these corrections will not be included in the SSH as the geophysical corrections for Sentinel-3 are not available at Level-1A and the information related to SSH is of no interest for the project.
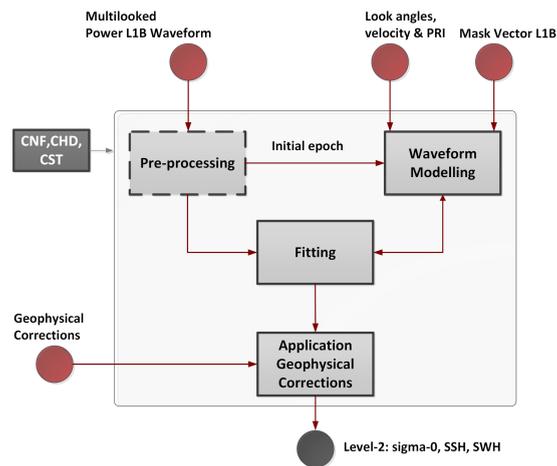
Figure 12: Block diagram of the L2 processor including the analytical SAR mode ocean retracker (CNF, CHD and CST stand for configuration characterization and constants' files).

3.3.2 Algorithm Definition:

<u>**Input Data:**</u>

- Sentinel-3A L1B products
- Configuration file
- Characterisation file
- Constants file

<u>**Output Data:**</u>

- SWH
- Sigma0
- SSH
- Quality flag
- Misfit (indication on how good the model fits the input data)

<u>Pre-processing:</u> provides an initial estimation of the epoch k_{epoch} based on a simple threshold retracker to ensure the convergence of the fitting procedure.

<u>Waveform modeling</u>: in charge of generating the theoretical model of the multi-looked SAR waveform, incorporating all the characteristics of the L1B processing.

This processing stage is integrated by four main processing stages: noise floor estimation, stack modeling, stack masking and multi-looking.

Noise floor estimation: a fixed window can be used to estimate the noise floor σ_n (before the leading edge of the waveform) or alternatively an adaptive window can be computed exploiting the derivative of the multilooked input waveform (first and last samples correspond to the range bin where the derivative of the input waveform is above a given threshold).

Stack modeling: the modelled stack should be built up using the different ***single-look power waveform*** defined according to model derived by Ray et al. 2015

$$P_{k,l}(P_u, k_0, H_s) = P_u \cdot B_{k,l} \cdot \sqrt{g_l(H_s)} \cdot [f_0(g_l \cdot (k - k_0)) + T_{k,l} \cdot g_l \cdot \sigma_s^2 \cdot f_1(g_l \cdot (k - k_0))]$$

Where

k range bin or index

l look or Doppler index associated to each beam that conforms the stack

P_u amplitude (fitting) parameter used in the final retrieval of the σ^0

k_0 epoch (fitting) parameter eventually providing SSH

H_s significant wave-height (fitting) parameter

σ_s normalized standard deviation of the surface height's probability density function (

$$\sigma_s = \frac{\sigma_z}{L_z} = \frac{H_s}{4 \cdot L_z}, \text{ with } L_z = \frac{c_0}{2 \cdot BW} \text{ as vertical resolution)}$$

$B_{k,l}$ and $T_{k,l}$ incorporate the information of the antenna pattern, antenna mis-pointing as well as the surface scattering model being assumed in the theoretical model. They are related, respectively, to the constant and first order terms of a Taylor approximation of the antenna and surface radiation patterns' product.

g_l models the dilation term, taking into account the instrument configuration, processing and the significant wave-height:

$$g_l = \frac{1}{\sqrt{\sigma_{ac}^2 + (2 \cdot \sigma_{al} \cdot \frac{L_x^2}{L_y^2} \cdot l)^2 + \frac{\sigma_z^2}{L_z^2}}},$$

where σ_{ac} and σ_{al} refer to the widths of the Gaussian functions that approximate the point target response in the across- and along-track dimensions; $L_x = \frac{\lambda \cdot H_{orb} \cdot PRF}{2 \cdot v_{sat} \cdot N_p}$ is the along-track resolution (with λ carrier wavelength, H_{orb} satellite orbit, v_{sat} satellite velocity, PRF pulse repetition frequency, N_p as the number of pulses in burst,); and

$$L_y = \sqrt{\frac{c_0 \cdot H_{orb}}{\alpha_R \cdot BW}}$$ across-track resolution (with α_R as the orbital factor).

$f_n(g_l \cdot k)$ for n=0,1 represent the range-dependent functions modulated by the Doppler-dependent dilation term g_l and represent the basis function of the model defined by

$$f_n(\eta) = \int_0^\infty (v^2 - \eta)^n \cdot e^{-(v^2-\eta)^2/2} dv$$

The estimated noise floor can be added as constant additive term to each Doppler beam to include the impact on the thermal noise in the modelled stack

$$S_{k,l}(P_u, k_0, H_s) = P_{k,l}(P_u, k_0, H_s) + \sigma_n.$$

Stack masking: once the modelled stack has been generated, the impact of any masking process carried out on L1B (wrapping effects due to geometry corrections, ambiguities masking,...) is accordingly incorporated in the model. To do so the L1B processor included in the DeDop platform provides the stack mask information for each output surface of the L1B: 1-D vector per surface, indicating, for each beam, the first range sample from which the mask is set to zero.

Multilooking: the final modelled multi-looked waveform is generated after incoherent averaging of the modelled stack, taking into account whether the samples artificially set to zero shall be considered or not in the processing (to be aligned with the procedure followed in the L1B multilook processing).

Fitting procedure: tries to converge to a solution in a least square error (LSE) basis by iteratively updating the modeled waveform used to fit the measured input L1B waveform.

Geophysical corrections: are applied to remove any environmental-dependent effects on the altimeter measurements. Geophysical corrections impairing the measured range are applied to the estimated sea surface height; these corrections will not be included in the SSH as the geophysical corrections for Sentinel-3 are not available at Level-1A and the information related to SSH is of no interest for the project.

3.4 ATBD-6: Amplitude Compensation and Dilation Compensation[4]

3.4.1 Function:

The aim of this algorithm is to perform an effective equalization of the different waveforms (one per Doppler beam) that conform the stack to the central zero-Doppler beam, leading to an improved signal-to-noise ratio and speckle noise reduction (as the different beams represent effectively additional trials of the reference central beam), see Makhoul et al. 2018. This leads to a simpler and faster retracker implementation as no stack modeling is required on the retracker itself. The output of the algorithm will provide also an estimation of the different geophysical parameters: SWH, σ_0 and epoch (SSH).

---

[4] This specific algorithm is not going to be part of the round robin exercise. It has been included for completeness on the ATBD as it is part of isardSAT research activities within the WP2000, and it may provide insights on how the optimized processing from L1A to L1B shall be considered.

The block diagram of ACDC algorithm is depicted in Figure 13. The main processing steps are:
- Amplitude compensation
- Dilation Compensation
- Multilooking
- Retracking
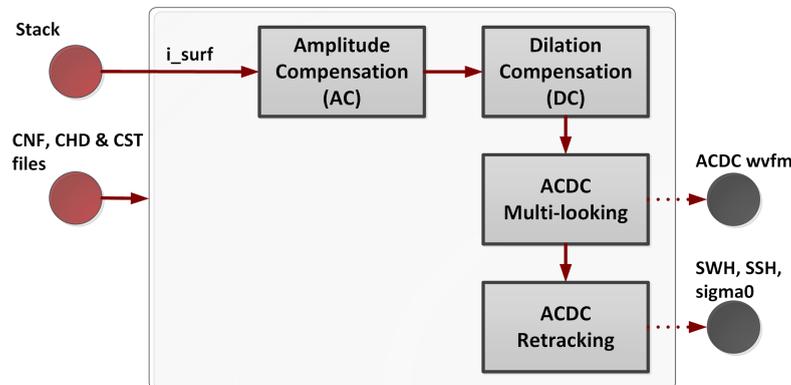
Figure 13: Block diagram of the ACDC algorithm.

3.3.2 Algorithm Definition:

Input Data:

- DeDop L1B-S product
- Configuration file
- Characterisation file
- Constants file
- Look Up Tables for range-dependent function

Output Data:

- SWH
- Backscattering coefficient σ_0
- SSH
- Quality flag
- Misfit (indication on how good the model fits the input data)

Amplitude compensation (AC): it carries out the compensation of the antenna/surface patterns as well as the so called Doppler-dependent dilation term g_l at stack level.

From the first order approximation of the SAR ocean single-look backscattered Ray et. al 2015:

$$P_{k,l} = P_u \cdot B_{k,l} \cdot \sqrt{g_l} \cdot f_0(g_l \cdot (k - k_0))$$

it can be noticed that the power in each range-Doppler cell is modulated not only by the antenna/surface patterns $B_{k,l}$ (constant term of Taylor expansion) as expected but also by the so called dilation term g_l[5]. This means that for those Doppler beams away from the central one there will be a widening of the waveform combined with an attenuation of the corresponding peak. Therefore, the amplitude compensation (AC) will consist of compensating these terms at stack level by means of

$$P_{k,l}^{AC} = \frac{P_{k,l}}{B_{k,l} \cdot \sqrt{g_l}} = P_u \cdot f_0(g_l \cdot (k - k_0))$$

In Figure 14 an example of the operation of the ACDC on the stack at the different processing stages is shown. It can be appreciated the equalization effect at stack level after AC (comparing top and bottom left figures).
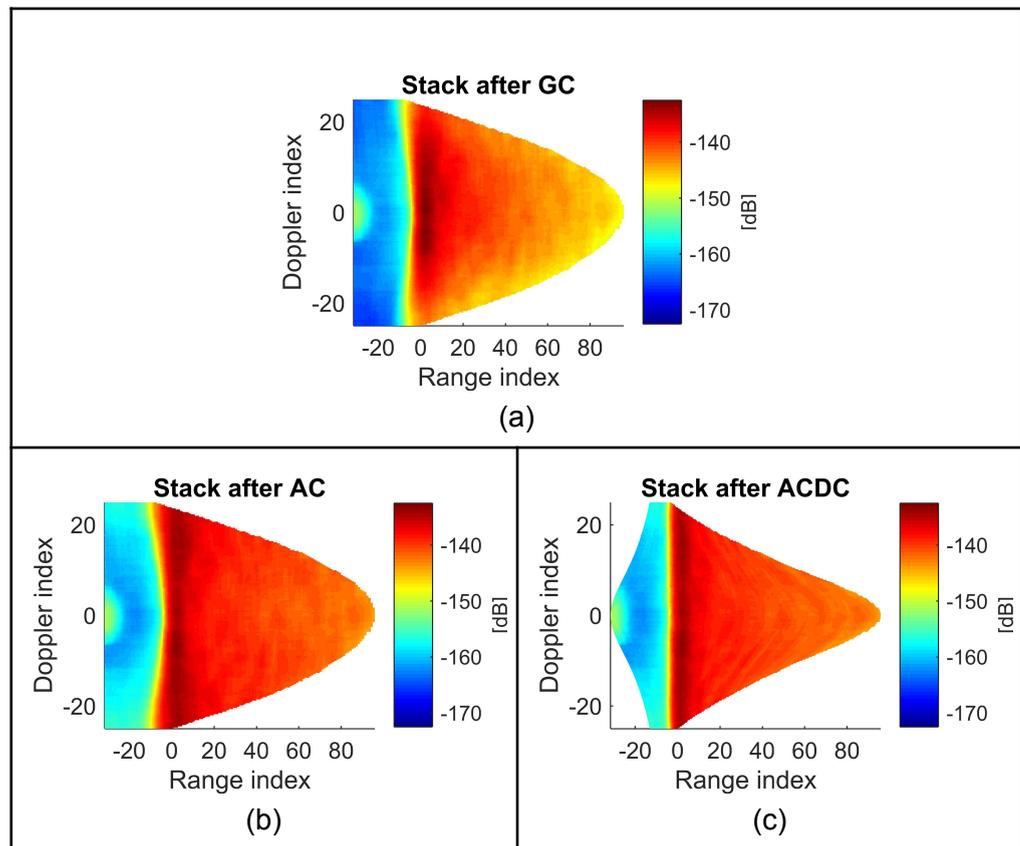
Figure 14: ACDC operation at stack level: (a) input stack to ACDC, after geometric corrections (GC) being applied, (b) after amplitude compensation and (c) after amplitude and dilation compensations (ACDC) [CryoSat-2 data has been used for the example][6].

---

[5] The definition of the dilation term can be found in the description of the conventional SAR ocean retracker implemented by isardSAT and described in section 3.3: ATBD-5.
[6] The input stack for the ACDC processing corresponds to the one after geometric corrections and stack masking being applied

<u>Dilation compensation (DC):</u>
The power in each Doppler beam after amplitude compensation can be regarded as a range-dilated version of the central beam (as shown in Figure 14b). The aim of this processing stage is to compensate for the widening or spreading of the beams away from the central one ($l = 0$), where the estimated Doppler frequency vanishes, so that the dilation-compensated range can be defined as $\kappa_{k,l} = \dfrac{g_l}{g_0} \cdot (k - k_0).$

The amplitude compensated (AC) waveform can be expressed in terms of the dilated range as
$P_{k,l}^{AC} = P_u \cdot f_0(g_0 \cdot \kappa_{k,l})$, leading to the ACDC stack as shown in Figure 14. In this way, ideally, all the power waveforms that conform the stack are the same and consequently the ACDC waveform is only function of the range axis.

<u>Multilooking:</u>
Since all the waveforms in the ACDC stack are realizations of the central waveform, the ACDC stack is re-organized as a 1-D vector. Then, an equivalent multilooked waveform is obtained by averaging those samples with nearly the same dilation-compensated (DC) range, exploiting a specific Gaussian weighting function $w(\cdot)$ centered at each DC range and with a given width δ (typically using half DC sample), that is,

$$\Psi_n^{ACDC} = \sum_{k,l} \frac{w(\kappa_{k,l} - n\delta) \cdot P_{k,l}^{ACDC}}{w(\kappa_{k,l} - n\delta)}\, .$$

<u>Retracking</u>:
The ACDC multilooked waveform can be fitted using a simplified model function as proposed by Ray et al. 2015b:

$$\Psi_n^{ACDC} = A \cdot f_0(g_0 \cdot (\kappa_n - \epsilon))$$

where the three fitting parameters are the amplitude A (related to the backscattering coefficient σ_0), the dilation term g_0 (from which SWH can be extracted) and the residual offset ϵ w.r.t initial epoch estimation k_0 (related to SSH). Before solving the optimization problem, an additive constant representing the thermal noise is added to the altimetric ACDC model waveform. This constant is estimated assuming the same noise floor power in all looks of the modelled ACDC stack. Hence, a window is applied within the leading edge of the multilooked power waveform with a size constrained to small variations of the gradient of the waveform according to a predefined threshold. The waveform parameters are estimated by fitting the model waveform to the data in the least squares sense. Boundary conditions that model physical constraints of the parameters are considered in the minimization problem. The constraint minimization problem is then solved numerically. Since the solution

is typically sensitive to the initial values of the parameters, several strategies have been examined and are described below.

The previous processing stages conform the core processing of the ACDC. In any case, the operation of the ACDC requires an initial estimation of the epoch (k_0) and the SWH to perform both the amplitude compensation and dilation compensation. Specific strategies has been followed to better allow the convergence of the ACDC method:
- A) ACDC will be run over the whole track several times (set by configuration parameter).
  - ○ For the first iteration over the whole track:
    - ■ The initial epoch value is extracted from a threshold retracker over the conventional Delay-Doppler L1B waveform (as a percentage on peak[7]); the SWH is extracted from configuration file, and it is set to a value typically above 5-m, to ensure ACDC convergence for low SWH cases. Then, ACDC iterates over the same surface (using initial epoch and SWH from previous estimates).

  - ○ For subsequent iterations over the whole track: the initial estimates for each surface are obtained directly from the smoothed version, using a running window, of the final estimates provided in the previous iteration over the track and no feedback between surfaces is considered in each iteration.
- A) ACDC algorithm runs once over the whole track.
  - ○ For the first surface, initial values of SWH and epoch are selected from the configuration file.
  - ○ For subsequent surfaces, a moving average is used to compute the initial estimates at each surface.

3.5 ATBD-7: LR-RMC PROCESSING (CLS)

First of all, a description of this algorithm is provided hereafter whereas this algorithm was initially not included in the list of algorithms provided by CLS. It has been added afterwards.
The Low-Resolution with Range Migration Correction (LR-RMC) mode is a newly ocean altimetry data processing showing promising results in many aspects: it provides no-correlated errors as observed in LRM data, mitigates swell impact on retrieval performances, and improves the measurement precision compared to unfocused SAR-mode over ocean. Note that this algorithm was added in a later phase and therefore was not announced in the ADP.

The three following sections describe the whole data processing chain, from the LR-RMC waveform generation, to high-level processing (sea-surface parameter estimation and the correction applied to significant waveheight estimates for correlated high-frequency errors).

L1A TO L1B LR-RMC PROCESSING

---

[7] Over open ocean scenarios the time of crossing 87 % of the peak of the SAR waveform can be considered as a fairly good estimation of the epoch of the leading edge.

3.5.1 Function:

This section deals with the processing scheme used for producing Sentinel-3 LR-RMC power waveforms at 20-Hz radar cycle rhythm. The figure below shows the main processes that are involved at this stage.
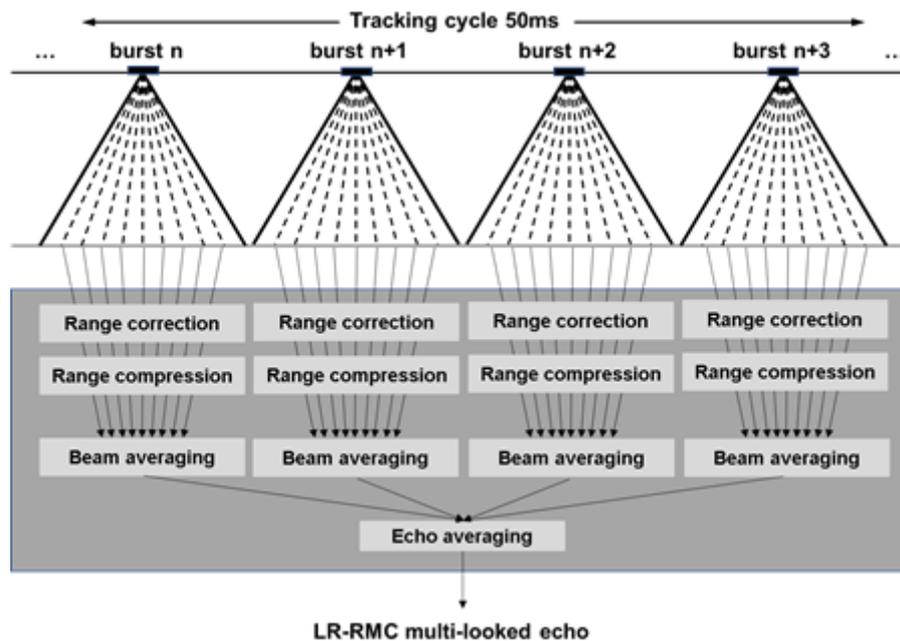

Figure 15 : Overview of the L1A to L1B LR-RMC processing scheme.

Similarly to unfocused SAR altimetry, the LR-RMC method coherently combines radar pulses in a burst to create a set of Doppler beams. But, unlike it, the LR-RMC method then sums all the beams contained in a radar cycle (4 bursts of 64 beams for the open-burst Sentinel-3-mode altimeter) to build a 20-Hz multi-looked waveform. The resulting footprint is much larger than that of the unfocused SAR altimeter (and as large as the illuminated area in conventional altimetry) allowing a better spatial average of the surface elevation to mitigate long ocean wave effects.

The LR-RMC technique takes advantage of a number of similarities in processing with the unfocused SAR altimeter approach (as described in Boy et al. [2017b]), which made its implementation relatively straightforward. This is even made easier thanks to major simplifications in the LR-RMC data processing scheme (no beam steering is needed and a shorter integration time is used to produce a mean multi-looked echo (approximately 50 times smaller than in SAR altimetry) thus minimizing possible errors in alignment and echo beam stacking, but also limiting possible surface movement effects). Despite this time duration reduction, the number of beams is as high as in SAR altimeter mode processing (4x64 averaged beams compared to 256 averaged looks in SAR altimetry), thus providing a noise reduction at least as good as, or even better than in SAR mode.

3.5.2 Algorithm Definition

INPUT:

- Sentinel-3A/B L1A products (also accounting for CAL1 and CAL2 correction data)
- Processing parameters file
- Altimeter characterization data file
- Constant data file

OUTPUT:

- Sentinel-3 LR-RMC L1B products:
    - Waveform
    - Waveform validity flag
- Model stack masking accounting for slant range correction

MATHEMATICAL STATEMENT:

Background

This processing has been first designed and used by Thales Alenia Space for in-flight assessing of Cryosat-2 data [Phalippou et Demeestere, 2011]. It has then been revisited by Boy et al. [2017a] as one of the most promising altimeter data processing solution to deal with long ocean waves issues while keeping high delay/Doppler measurement capability in terms of precision. Subsequent studies carried out with Sentinel-3 data have proved that this newly processing approach not only limits swell impact on retrieval performances but also exhibits improved ocean measuring performance compared to unfocused SAR mode [Boy et al., 2017a]. To illustrate these results, the figure below compares the LR-RMC SWH noise with that derived from the unfocused SAR mode. It can be seen that the LR-RMC SWH noise does not depend on the azimuth angle nor on the mean wave period, and is additionally far below the SAR SWH noise level.
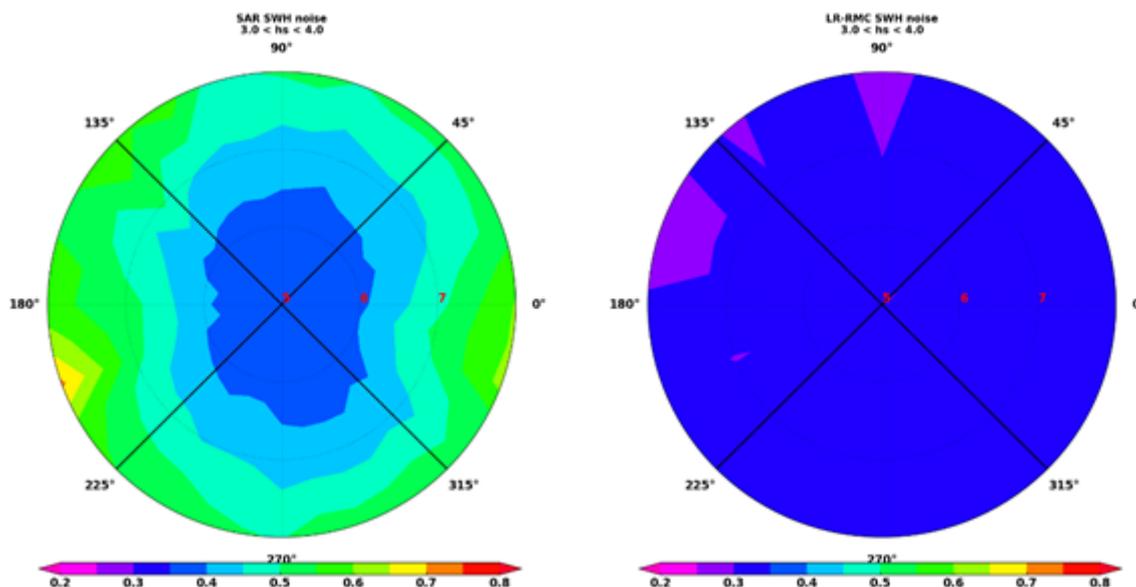
Figure 16: Bin-averaged SWH noise for unfocused SAR (left panel) and LR-RMC (right panel) processing against mean swell period (radial distance, in seconds) and azimuth angle (angle between the satellite flight direction and the mean swell direction) for 3 m < SWH < 4m.

Main steps of the processing

The main steps of the processing are the following:

The first on-ground processing step consists in applying an **along-track Fast Fourier Transform on each burst** of a given nadir cycle, similarly to what is done in the unfocused SAR approach. This method coherently combines radar pulses from a burst to produce a set (also called fan) of Doppler beams looking toward different directions along the satellite track (at equally spaced angles across the radar antenna aperture).

The Doppler beams fan is **corrected from Doppler centroid shift** (due to the radial velocity of the spacecraft), to keep it centered on the surface location of the satellite sub-point (i.e. the nadir point).

Then the Doppler beams are **range migrated** with respect to the nadir beam (i.e. correction compensating for the slant-range migration, mean sea surface slopes and curvatures, tracker-range misalignment within a radar cycle and the Doppler shift in range) and **range compressed**.

Finally, **all the range-aligned beams are summed incoherently** to form a Doppler echo (one for each nadir cycle).

LR-RMC OCEAN NUMERICAL RETRACKER

3.5.3 Function

To perform the ocean numerical retracking on the LR-RMC altimeter waveforms (main band), i.e. to estimate the altimetric parameters (swh, epoch, amplitude).
The model is designed for retracking LR-RMC waveforms over ocean surfaces only.

3.5.4 Algorithm Definition

INPUT:

- Waveform:
    - Waveform
    - Waveform validity flag
- Platform-derived off-nadir angles:
    - Roll angle
    - Pitch angle

- Orbit:
    - Orbit altitude (20-Hz)
- Altimeter instrumental characterization data:
    - Altimeter instrumental characterization data for the preparation of data for the ocean retracking (Point Target Response and Low Pass Filter)
    - Abscissa of the reference sample for tracking
    - Sampling interval of the analysis window
    - Antenna beamwidth
    - Ratio between the PTR width and the sampling interval of the analysis window
- Initial value of epoch given by the surface height from the OCOG retracker
- Model stack masking (from L1b data) accounting for slant range correction
- Universal constants (SAD):
    - Light velocity
    - Earth radius

OUTPUT:

- Epoch: τ
- Significant waveheight: SWH
- Amplitude: P_u
- Thermal noise level: P_n
- Number of iterations
- Mean Quadratic Error

Quality flag (valid / invalid)

MATHEMATICAL STATEMENT:

Background

The aim of this numerical retracking algorithm is to make the measured LR-RMC waveform coincides with a power echo model, according to weighted Least Square Estimators derived from Maximum Likelihood Estimators, to retrieve the altimetric parameters: epoch, swh, amplitude. But in contrast to conventional analytical approach, the numerical retracking algorithm uses pre-simulated echo models which have the major advantage of accounting for the actual features of the instrument measured on-ground, before launch (e.g., the real range impulse response, the real antenna pattern), or any instrumental ageing issues that may be characterized through periodic in-orbit calibration activities. This approach is more robust than analytical ones, particularly when faced with atypical observations that are difficult to put into equations.

Partial derivatives required by the algorithm are thus computed in a numerical way.

For each 20-Hz measurement, the parameters to be estimated are:
τ　　　: the epoch
SWH　: the significant waveheight

P_u : the amplitude

P_n : the thermal noise level (estimated from an arithmetic average of samples of the first plateau)

The echo model database depends on the platform-derived off-nadir angles (roll and pitch) and the orbit altitude of the satellite. They are required on input of the LR-RMC numerical retracking algorithm to perform the three altimetric parameters estimation.

Basic principle

The problem to solve is the estimation of a set of *N*=3 parameters $\theta = \{\theta_1 = \tau, \theta_2 = swh, \theta_3 = P_u\}$. The system to solve results from the maximization of the logarithm of the likelihood function $\Lambda(\theta)$, i.e. from the system:

$$C(\theta) = \nabla[-Ln(\Lambda)] = 0 \tag{1}$$

where C is the total cost function and ∇ is the gradient function.

This system is reduced to weighted Least Square Estimators, and is equivalent to set the Least Square function $\nabla\chi^2$ to 0, where the merit function χ^2 is defined by:

$$\chi^2 = \sum_i \left(\frac{V_i\_Vm_i}{\sigma_i}\right)^2 \tag{2}$$

where V represents the measured waveform, and where the weighting function is $\{\sigma_i\}$ = $\{Vm_i\}$.

This system may also be represented by the following set of N_θ equations:

$$\sum_i \left(\frac{Vm_i - V_i}{\sigma_i^2}\right) \cdot \frac{\partial Vm_i}{\partial\theta_k} = 0 \tag{3}$$

An iterative solution is obtained by developing the total cost function in a Taylor series at the first order about an initial set $\theta_0 = \{\theta_{01} = \tau_0, \theta_{02} = swh_0, \theta_{03} = P_{u_0}\}$ of estimates:

$$\theta_{n+1} = \theta_n - g.\varepsilon_\theta \tag{4}$$

with: $\varepsilon_\theta = (BB^\mathsf{T})^{-1}BD$ (valued to the current values θ_n)

B,D are the partial derivatives and residuals matrix:

$$B_{ki} = \frac{1}{\sigma_i} \cdot \frac{\partial Vm_i}{\partial\theta_k}, \quad D_{i1} = \frac{1}{\sigma_i} \cdot (Vm_i - V_i) \tag{5}$$

and where g is a loop gain (positive value, unique to the parameter being estimated).

Using $\{\sigma_i\}$ = $\{Vm_i\}$, the Least Square Estimators method described above would put the most weight on the regions with the least power, i.e. on the regions with the least information regarding the parameters to be estimated. For this reason, the weighting function is superseded by a factor constant over a waveform ($\{\sigma_i\}$ = s). In order to normalize the residuals ($\{Vm_i-V_i\}$), this factor s is set to the current estimate of the amplitude.

The derivatives of the mean return power *B* are approximated by a finite difference computed numerically as following:

$$\frac{\partial \mathrm{Vm}_i}{\partial \theta_k} = \frac{\mathrm{Vm}_i(\theta_k + h_k) - \mathrm{Vm}_i(\theta_k)}{h_k}$$

(6)

where models *Vm* using the current estimation vector θ_n are directly taken from the echo model database.

Main steps of the processing

The algorithm consists of the following functional units:

- To load and construct the LR-RMC altimeter echo model:

For each data segment (~1s time interval currently used in CNES Sentinel-3 Processing Prototype), a power echo model involved in the estimating process is retrieved from the database according to the mean orbit and platform off-nadir angle values (see figure below). The extracted model is further convolved with the measured PTR.
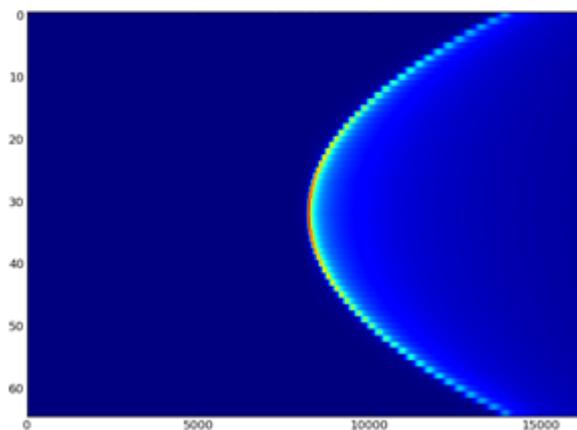

Figure 17: Simulated model of Doppler echo beams oversampled in range. The apex of the hyperbola is placed at the centre of the range window.

The map of simulated Doppler beams is truncated for those samples that are considered out of the altimeter range window, with respect to the initial value of the epoch (estimated by the OCOG retracking).
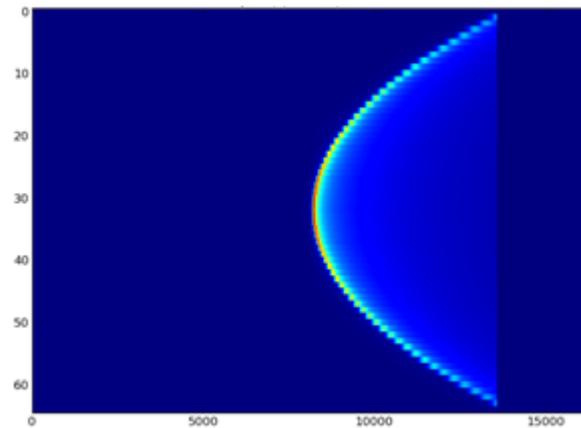
Figure 18: Simulated model of Doppler echo beams shortened in range.

The next stage consists in correcting in range the Doppler beams to align them to each other. Shifts in range are performed by a convolution operation with a Dirac delta function.
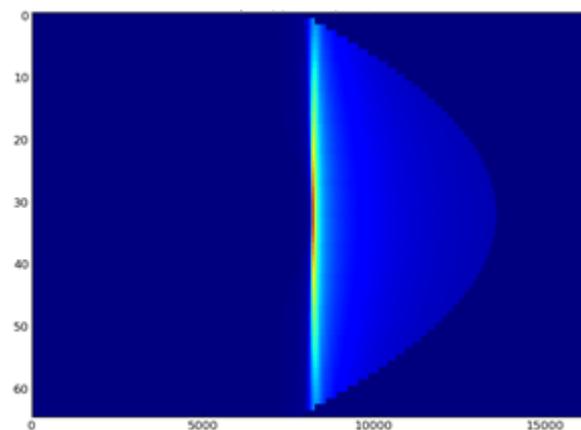
Figure 19: Simulated model of Doppler echo beams after range alignment.

Finally, all squared Doppler beam waveforms of the map are summed. The constructed LR-RMC power echo is the numerical model that is used to process the data segment.
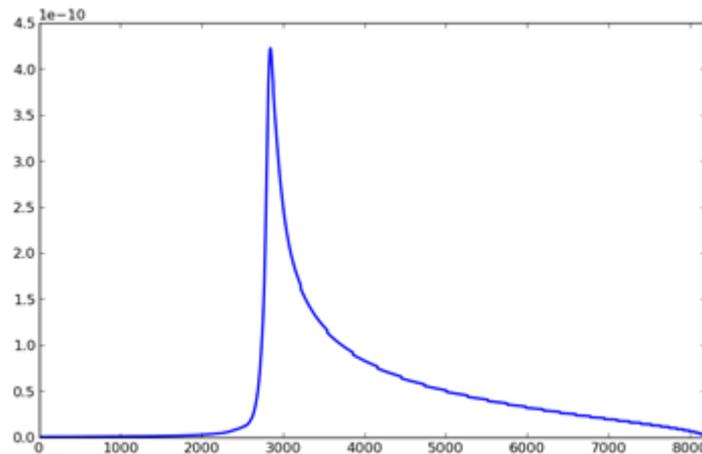
Figure 20: The resulting LR-RMC power echo model

- Identification of the waveform validity:
   - The validity of the waveform is determined from the input waveform quality information. The retracking is then performed only if the input waveform is valid.
- Thermal noise estimation:
    - The thermal noise level (P_n) is computed from an arithmetic average of samples of the first plateau (in a range of gates defined as processing parameters).
- Estimation (weighted Least Square fit):
    - The fine estimates of the epoch (τ), the significant wave height (SWH) and the amplitude (P_u) are derived from the iterative process defined previously, which is initialized from the value τ_0 (as defined above) and the default values σ_{c0} and P_{u0} (input processing parameters) for each waveform.
    - To compute the LR-RMC altimeter echo model with the parameters $\{\tau, SWH, P_u\}$, the echo model is first convolved with a Dirac delta function at the epoch τ. Then the shifted echo model is convolved with a sea surface height distribution (defined by the swh value). Finally, the P_u gain is applied and the echo model is sub-sampled.
    - This estimation process is stopped when the value of the mean quadratic error (MQE) between the normalized waveform (i.e. the waveform from which P_n is removed and weighted by $1/P_u$) and the corresponding model built from the estimates is stable enough, with a minimum number of iterations performed, or when a maximum number of iterations is reached.
- Set the quality flag:
    - The estimates with a MQE below a certain value are valid and must be kept. The others are considered non-valid and have to be edited. Based on this criterion, a quality flag provided at 20 Hz is set at "0" when the estimate is valid, otherwise is set at "1" (0=good;1=bad). This quality flag is to be used for the data analysis at 20Hz and to compress them at 1Hz.

Comments

- As mentioned in section "Mathematical statement", an echo model database is computed off-line by a numerical simulator that mimics the altimeter response and follows closely the ground data processing that is employed for generating waveform data. For the Cryosat-2 unfocused SAR data processing performed by CNES [Boy et al., 2017b], a fully numerical and adaptive simulator developed by Desjonquères et al. [2012] were used. It consists in simulating a point-by-point radar response on a gridded surface (with no limitation of resolution) then in applying a specific Delay/Doppler development to ultimately generate an unfocused SAR power return waveform model. The echo model database is computed by varying the simulation parameters (satellite altitude and roll/pitch angles), one parameter at a time, in a range of values and with a step size that have been chosen to ensure the accuracy and precision of the estimates. Theoretical or measured antenna pattern can be used taking into account mispointing in both axis. Theoretical or measured impulse responses can be used too. The following figure illustrates the different steps of the echoes simulator as defined by Desjonquères et al. [2012]. LR-RMC echo models were generated using the same simulator [Boy et al., 2017a].
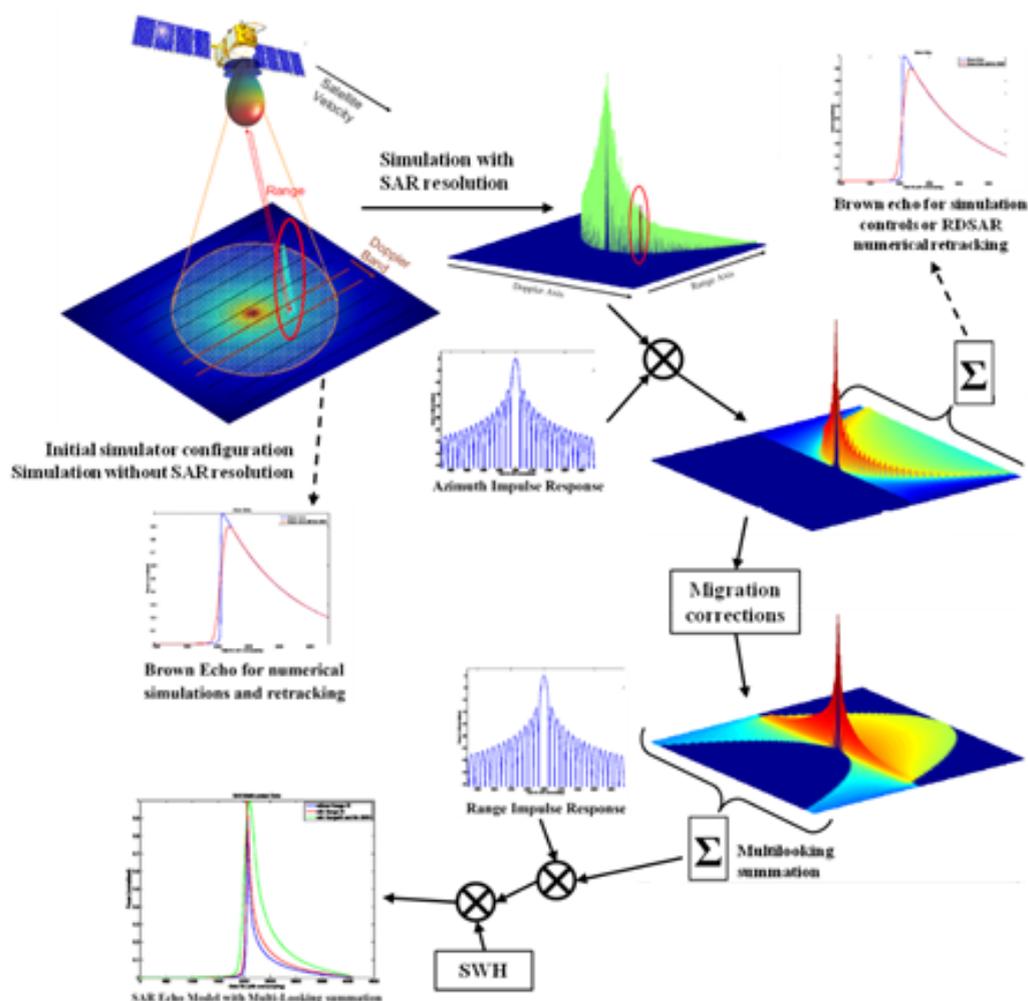

Figure 21: SAR altimeter echoes simulator (from Desjonquères et al., 2012).

- To ensure consistency between level-1 and level-2 processing, any mask applied in level-1 processing should be applied to the delay/Doppler map model as well.

INTRA-1HZ CORRECTION FOR LR-RMC RETRACKER

3.5.5 Function

To compute 20-Hz corrected Ku-band ocean significant waveheight for correlated high-frequency errors

3.5.6 Algorithm Definition

INPUT:
- 20-Hz Ku-band ocean significant waveheight
- 20-Hz Ku-band ocean range
- validity flag

OUTPUT:

- 20-Hz corrected Ku-band ocean significant waveheight

MATHEMATICAL STATEMENT:

An empirical high-frequency correction based on range noise is applied on nominal 20-Hz SWH. The approach is similar to the one defined by Zaron and DeCarvalho [2016] to correct sea surface height estimations.

LOW RATE SWH ESTIMATES

3.5.7 Function

To compute a compressed SWH estimate from 20-Hz estimates.

3.5.8 Algorithm Definition

INPUT:
- 20-Hz Ku-band ocean significant waveheight

- quality flag

OUTPUT:

- 1-Hz Ku-band ocean significant waveheight
- Standard deviation
- Map of valid estimates
- Validity of the compressed estimate

MATHEMATICAL STATEMENT:

The processing steps are as follows:

- To identify the 20-Hz measurements to be compressed, accounting for the mean quadratic error issued from the ocean retracking (quality flag).
- To compute the compressed estimate of SWH from the set of valid 20-Hz estimates using an arithmetic averaging (note that outliers are detected and rejected within the compression process if their value departs from the mean value by more than a minimum value of the standard deviation).
- To compute the compressed estimate of SWH and the standard deviation for the last set of selected estimates.

4. Algorithms for Synthetic Aperture Radar Processing

4.1 ATBD-8: CWAVE_S1-WV

The developed empirical algorithm consists of two parts: CWAVE_EX (extended CWAVE) based on widely known approach and additional machine learning postprocessing. The combined algorithm is designed for processing of S1 Level-1 SLC Wave Mode (WV) data.

The algorithm consists of two steps for estimation of sea state parameters: the initial step is based on classical CWAVE parameters related by linear regression model function (Schulz-Stellenfleth et al., 2007) and extended with additional features. The second postprocessing step uses machine learning, i.e. the support vector machine technique (SVM), to improve the accuracy of the initial results. In this way, the accuracy of initial SWH estimated using linear regression with ~0.35m accuracy for S1 WV (CMEMS-hindcast validation) has been improved to ~0.25m accuracy by SVM postprocessing.

The method was trained and validated with CMEMS 3h (temporally interpolated) model results and additionally validated against 50 km collocated NDBC buoys. Worldwide were found 61 buoys with significant wave height SWH records for 2015-2021.

The algorithms for sea state parameter estimation for different SAR data have been developed and integrated into the Sea Sate Processor (SSP) for fully automatic processing for near real time (NRT) services. The current version was developed initially for X-Band TerraSAR-X imagery (StripMap, Spotlight, Pleskachevsky et al., 2016), later extended for S1 IW imagery (Pleskachevsky et al., 2019) and adopted finally for S1 WV SLC products (Pleskachevsky et al., 2021).

The processing is a part of an NRT service chain operated at the DLR Ground Station Neustrelitz. It allows the processing and delivery of sea state products within 5min to 30min after image acquisition. The processing chain has been constantly improved. The infrastructure allows also automatic and rapid processing of historical archive data. This timing includes about 3min to 12min for data reception, decoding and SAR image processing (level L0 and L1 processing), followed by sea state estimation and finishing with generation and delivery of wave products (L2 processing). The priority of the algorithm design is an automatic, fast and robust raster processing of SAR acquisitions independent from wave patterns, which means it is also applicable when only clutter is visible in the SAR images. The SSP runs daily at the ground station for Sentinel-1 IW scenes in North and Baltic Sea. Figure 22 provides an overview of the whole algorithm implementation.
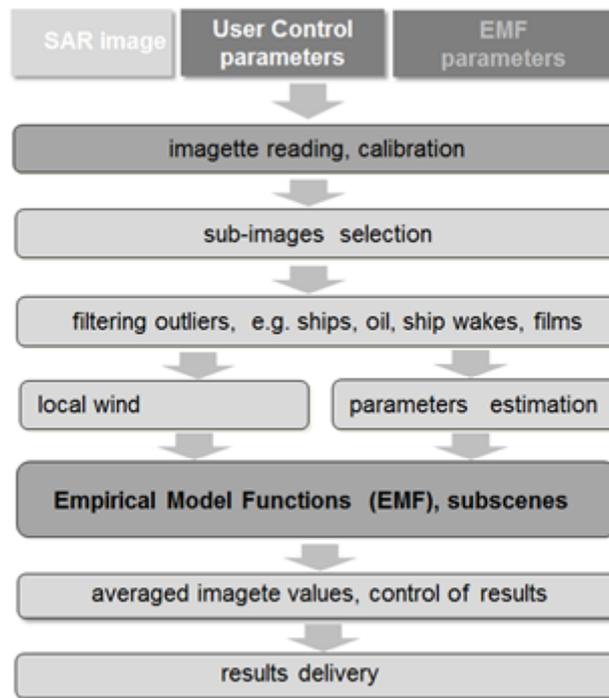
Figure 22: Flow chart of the Sea State Processor (SSP) Infrastructure for generation of sea state products.

4.1.1 Function:

The model functions are based on analysis of subscenes and allow direct significant wave height (*SWH*) estimation from image spectra without transferring into wave spectra. The model functions are based on integrated image spectra parameters as well as local wind information estimated by the CMOD geophysical model functions. Additionally, a texture analysis based on Grey Level Co-occurrence Matrices (GLCM) is performed and the extracted textural features are integrated in the model function. The processing includes three main steps:

1. Data preparation: reading, calibration and artefact/outlier pre-filtering
2. Feature extraction & model function application
3. Control of results

1) Data preparation: reading, calibration and artefact/outlier pre-filtering

The reading and calibration of Sentinel-1 WV SLC data is in detail described in the Sentinel-1 Product Specification. In order to obtain uniformly scaled intensity values, which are representing comparable backscatter characteristics of the ocean surface on diverse Sentinel-1 WV acquisitions, the images must be radiometrically calibrated.

The pre-filtering of artefacts and outliers is important to obtain uncontaminated image regions, because contaminated regions interfere with the extraction of image features of sea state. A direct application of the Empirical Model Function (EMF) to the features extracted from a subscene often leads to inaccuracies in SWH estimation with outliers in the range of

meters. The sources of these errors are in the first place a number of natural and man-made artefacts like current boundaries, wind streaks, ships, wind farm constructions or buoys. They can be divided into two classes: radar echo is much stronger than background backscatter (e.g. ships) or radar echo is much weaker than background backscatter (e.g. oil slicks). A pre-filtering procedure to recognize and possibly remove the signals not produced by sea state before the analysis is applied by replacing the outlier pixels in the current sub-subscene by the mean value of the subscene.

2) Feature extraction & model function application

The core of the method is a linear regression model function based on the widely known CWAVE approach (Schulz-Stellenfleth et al., 2007, Stopa and Mouche, 2017). However, in order to reach higher accuracy not only for Hs but also for the other estimation parameters, i.e. wave periods (total integrated parameters) and partial integrated parameters like swell and wind-sea wave heights, a series of procedures (e.g. pre-filtering, artefact filtering, smoothing etc.) are included and a number of additional SAR features are involved (e.g. GLCM, Image Spectrum integrated for different wavelength domains), which are partially published in Pleskachevsky et al., 2016 and Pleskachevsky et al., 2019.

The sea state parameter's estimation is based on NRCS sub-scenes analysis. To get more stable results, each S1-WV imagette of 20km×20km extent is processed several times by sub-images using a sliding window of ~4.6 km×4.6 km (FFT-1024) extent to get averaged values for each estimated SAR feature, while outliers are filtered based on a simple outlier analysis. Since the values of many SAR features differ between wv1 and wv2 imagettes, two independent functions for both tracks were developed with a general tendency of lower accuracy for wv2.

Five SAR feature types are involved for tuning of the model function:

- **type-1:** NRCS and NRCS statistics (variance, skewness, kurtosis, etc.).
- **type-2:** geophysical parameters (wind speed using CMOD algorithms).
- **type-3:** Grey Level Co-occurrence Matrix (GLCM) parameters (entropy, correlation, homogeneity, contrast, dissimilarity, energy, etc.).
- **type-4:** Spectral parameters based on image spectrum integration of different wavelength domains (0-30m, 30-100m, 100-400m, 400-2500m etc.) and spectral width parameters (Longuet-Higgins, Goda-parameter).
- **type-5:** Spectral parameters of *ISP* defined in Schulz-Stellenfleth et al., (2007) using orthonormal functions and cut-off wavelength estimated using autocorrelation function (ACF).

The whole list of SAR features included in the tuning procedure is shown in Tab.1. Therein, features selected according to Pleskachevsky at.al 2019 were extended with already known features (*marked italic*) and new features (***bold italic***). The usage of the new features is neither published yet for S1 IW nor for WV and will be described in Pleskachevsky et al., 2021.

Tab. 1: First-order SAR features used in CWAVE_EX model functions (57 features).

type description	feature description	symbol
1. NRCS and NRCS statistics	1.1. Mean Intensity of subscene scaled	*MI*
	1.2. STD of NRCS	*STD*
	1.3. Normalized variance	*nv*
	1.4. Variance of normalized NRCS	*Nv*
	1.5. Skewness	*skew*
	1.6. Kurtosis	*kurt*
	1.7. Discription in publication: Pleskachevsky et al., 2021	N_{HV}
	1.8. Discription in publication: Pleskachevsky et al., 2021	*INT*
	1.9. Discription in publication: Pleskachevsky et al., 2021	*INT_LOG*
2. Geophysical	2.1. Wind using CMOD	U_{10}
3. GLCM, (grey level co-occurrence matrix) feature analysis	3.1. GLCM-mean	*GLCMM*
	3.2. GLCM-variance	*VAR*
	3.3. GLCM-entropy	*ENTROPY*
	3.4. GLCM-correlation,	*CORR*
	3.5. GLCM-homogeneity	*HOMOGEN*
	3.6. GLCM-contrast	*CONTRAST*
	3.7. GLCM-dissimilarity	*DISSIMIL*
	3.8. GLCM-energy	*ENERGY*
4. Spectral-A	4.1. Integrated Energy for *k*-domain 0.01-0.21 corresponds to wavelength 30-2000m	E_{IS}
	4.2. Energy integrated with noise deduction (No Noise)	E_{NN}
	4.3. Energy Integrated with dividing each spectral *k*-bin by k^2	E_K
	4.4. Integrated Energy of a spectrum for wavelength 0-30 m	E^{30}
	4.5. Integrated Energy of a spectrum for to wavelength 30-100 m	E^{100}

	4.6. Integrated Energy of a spectrum for wavelength 100-400 m	E^{400}
	4.7. Integrated Energy of a spectrum for wavelength 400-600 m	E^{600}
	4.8. Integrated Energy of a spectrum for wavelength 6000-2000	E^{2000}
	4.9. *Integrated Energy of a spectrum for wavelength >2000 m*	$E^{>2000}$
	4.10. Spectrum Noise inside of *cut-off* domain of the spectrum	N^{S}_{in}
	4.11. Spectrum Noise outside of *cut-off* domain of the spectrum	N^{S}_{in}
	4.12. Energy max in the spectrum	E_{MAX}
	4.13. *Longuet-Higgins parameter*	P_{LH}
	4.14. *Goda parameter*	P_{G}
	4.15. *Discription in publication: Pleskachevsky et al., 2021*	*CONV*
	4.16. *Discription in publication: Pleskachevsky et al., 2021*	*REL*
	4.17. *Discription in publication: Pleskachevsky et al., 2021*	*Syx*
5. Spectral-B	5.1 – 5.20. *20 parameters as product of normalized image spectrum and 20 orthonormal functions*	$S_1 – S_{20}$
	5.21. *Cutoff by ACF (Auto-Correlation-Function)*	*λc*

The set of CWAVE_EX model functions are based on a linear regression:

$$W_N = A_{N_0} + \sum_{i=1}^{N_f} A_{N_i} s_i \qquad (2)$$

where denotes the sea state estimation parameter $N=1,2…N_p$ (for $N=1$, for $N=2$, for $N=3$, etc.). The whole list of eight considered sea state parameters ($N_p=8$) is shown in Tab.2. N_f is the number of all considered SAR features and for $i=0$ is a constant.

The SAR feature matrix **S** can be written as

S=(1, **S$_A$, S$_B$, S$_C$**) $\qquad (3)$

and consists of:

- first-order parameters S_A; features estimated from SAR image including all 5 types (direct relationship between features and required sea state parameters), see Tab.1.
- Inverse features $1/s_i$ S_B
- combination between first-order parameters in a quadratic form S_C

While the number of S_A features constantly remains 57 (see Tab.1, primary features), for S_B and S_C only combinations improving the resulting RMSE by at least 0.001m were selected. Finally, S includes 130 features.

Since the SAR features differ by several orders of magnitude, their use in a linear combination leads to an underrepresentation of features with small values. Thus, a normalization of features was applied to obtain the feature-normalized matrix S^n:

$$S^n = \frac{S - \langle S \rangle}{std(S)}$$

(4)

where $\langle S \rangle$ is the mean value of S and $std(S)$ is the standard deviation of S over all analysed samples.

The solution for Eq.2 is the standard quadratic RMSE minimization for parameter matrix w_N, and the ground truth matrix W_N (collocated model results), solved using singular value decomposition technique (SVD).

$$RMSE = \sqrt{\frac{1}{n}\left(w_N - W_N\right)^2}$$

(5)

Tab.2 : Estimation parameters

N	Symbol	Description	unit	integration
1	H_S	significant wave height	m	total
2	Tm_1	first moment wave period	sec	total
3	Tm_2	sec. moment wave period	sec	total
4	Tm	Mean wave period	sec	total
5	$H_S^{swell-1}$	sig. wave height swell dom. system	m	partial
6	$H_S^{swell-2}$	sig. wave height swell second system	m	partial
7	H_s^{wind}	sig. wave height windsea	m	partial
8	T^{wind}	mean period wind sea	sec	partial

3) Machine learning postprocessing

The accuracy using linear regression amounts to RMSE of ~35 cm (CMEMS). The stored first-order features have been used for reprocessing (postprocessing) SWH using machine learning technique improving RMSE to ~25 cm. The sea state reprocessor SSR reads the files with stored features (ID_results), output files with stored SWH (ID_sea-state), extracts the new SWH value and replaces them in output files.

As machine learning instrument, the support vector machine (SVM) technique was applied using an epsilon-SVR regression function and radial basis function as kernel-type.

As input, the first-order SAR features were used (Tab.1), extended by three additional features:

- first-guess *SWH* from linear regression solution.
- precise incidence angle (degree, third decimal place)
- flag identifying the satellite (0 for S1-A and 1 for S1-B).

More details for SVM constellation, values of cost, gamma and tolerance parameters can be found in Pleskachevsky et al., 2021.

4) Control of results

After an imagette is processed, the statistics of parameters for all imagette subscenes are used for result controlling. Additional to sea state parameters and geo-coordinates, SWH quality (swh_quality), uncertainty (swh_uncertainty) and rejection flag (swh_rejection_flag) are stored (see Tab.2).

Tab.2: Control of results: quality, uncertainty and flag

swh_uncertainty	RMSE calculated from CMEMS model colocations
swh_quality	quality of C band SAR significant wave height measurement: 0 undefined; 1 bad; 2 acceptable; 3 good
swh_rejection_flags	consolidated Significant Wave height quality flags

4.1.2 Algorithm Definition:

Input Data:

- S1 WV SLC products for processing using linear regression
- Stored SAR features and results (SWH) for reprocessing using SVM

Output Data:

- Primary:
    - SWH
    - Quality Flag

- Secondary:
    - mean period Tm0
    - first moment wave period Tm1
    - second moment wave period Tm2
    - swell dominant system wave height Sw1
    - swell secondary system wave height Sw2
    - Windsea wave height Sww
    - Windsea period Tmw

Pleskachevsky, A., Jacobsen, S., Tings, B.: Multiparametric sea state fields from Synthetic Aperture Radar for maritime situational awareness. 2021, (Submitted)

Pleskachevsky, A., Jacobsen, S., Tings, B., Schwarz, E.: Sea State Parameters from SAR for Maritime Situational Awareness. IJRS, Vol. 40-11, pp. 4104-4142., 2019.

Pleskachevsky, A., W. Rosenthal, Lehner, S.: Meteo-Marine Parameters for Highly Variable Environment in Coastal Regions from Satellite Radar Images." Journal of Photogrammetry and Remote Sensing, Vol. 119, pp. 464-484., 2016.

Stopa, J., Mouche, A.: Significant wave heights from Sentinel-1 SAR: Validation and Applications. JGR, Vol., 122, pp. 1827-1848., 2017

Schulz-Stellenfleth, J., König, Th., Lehner, S.: An empirical approach for the retrieval of integral ocean wave parameters from synthetic aperture radar data. JRL, Vol. 112, pp. 1-14., 2007

Schlembach, F., Passaro, M. , Quartly, G.D. , Kurekin, A. , Nencioli, F. , Dodet, G. , Piollé, J.-F. , Ardhuin, F. , Bidlot, J. , Schwatke, C. , Seitz, F. , Cipollini, P., Donlon, C.. : Round Robin Assessment of Radar Altimeter Low Resolution Mode and Delay-Doppler Retracking Algorithms for Significant Wave Height. Remote Sens. 2020, 12, 1254.

4.2 ATBD : Sentinel-1 wave mode optimal training

This algorithm corresponds to previous ADP-8

4.2.1 Function:

The algorithm aims at estimating significant wave height and spectral parameters, even in cases where SAR imaging mechanism becomes non-linear. In scenarios where SAR image spectra become distorted, statistical approaches are used to estimate wave conditions. These statistical models are trained to predict quantities of interest from distorted SAR images. The typical approach is to train using a parameterized physics model of global wave spectra, limiting their accuracy to that of parameterized physics model. This work improves the accuracy of statistical methods for predicting significant wave height from SAR by leveraging satellite altimeter observations. We construct a data set of over 700,000 colocations of five altimeter missions with the two identical Sentinel-1 SARs, which we use to train a deep neural network regression model. This improvement will enable sea state information to be obtained in environments that would not be possible with current SAR analysis methods.

4.1.2 Algorithm Definition:

Input Data:

- S1 WV SLC products
- Intercalibrated multisatellite altimeter wave height dataset.

Output Data:

- Primary:
    - SWH
    - Quality Flag
- Secondary:
    - mean period of the first 3 most energetic wave systems
    - mean direction of the first 3 most energetic wave systems
    - mean wavelength of the first 3 most energetic wave systems

MATHEMATICAL STATEMENT:

The general procedure is to find S-1 acquisitions with small differences in time and space compared to buoys and altimeter SWH observations. In the case of altimeters, the satellites must measure the same patch of ocean within reasonably small time and space constraints. In the case of moored buoy observations, S-1 acquisitions must be reasonably close to the buoy location and time of buoy measurements. We set coarse constraints to create the original dataset with time differences less than 3 hours and space differences less than 300 km. We then explore adequate time and space constraints by developing the deep learning models that use this information as input.

Based on the 760,000 collocated data points, 60% of the dataset is used for training (the training set), 20% for tuning "hyper"-parameters such as the network architecture, learning rate, stopping-criteria, etc. (the validation set), and the final 20% for independent model evaluation (the test set). Here we present the first application of deep learning to the problem of predicting Hs from SAR acquisitions based on a training dataset from homogeneous and qualified multi-altimeter observations.

Most inputs to the model, namely the 20 non-dimensional orthogonal coefficients, the distance between the SAR satellite and altimeter satellite, and the time difference between the satellites, are standardized to have a zero mean and variance of one. The incidence angle of the SAR image is first used to split into two groups for incidence angles of around 23 degrees (WV1) and around 37 degrees (WV2) respectively, and then normalized separately for each group in a similar manner as mentioned above. A few input parameters however were processed differently. The latitude and longitude were encoded as four new features: sin(phi), cos(phi), sin(theta), cos(theta). This prevented boundary effects at the poles and the international dateline. A similar encoding was used for the time-of-day feature, were time t was encoded between [-1; 1] with the function f(t) = 2sin(2t/48))-1. Finally,

whether the SAR measurements were taken by the S-1A or S-1B satellite were both represented as binary labels.

The neural network architecture has twelve hidden layers of 64 units (with the Rectified Linear Unit (ReLU) activation function) and an output with two outputs y1; y2 that parameterize a heteroskedastic Gaussian distribution N(y1; g(y2)) where the non-linear function g ensures that the variance is positive, and is defined as g(x) = x for x > 0 and g(x) = 1=(1 - x) for x < 0. The model is trained to maximize the conditional log-likelihood of the targets using the Adam optimizer (Kingma & Ba, 2014). Training is done on mini-batches of size 1024, with an initial learning rate of 0.003, that starts smoothly decaying after after 300 epochs with a decay rate of 0.0005. The loss on the validation set is monitored during training, and training is stopped after no improvement in validation loss is seen for 100 epochs, or after 1000 epochs, whichever comes first. These model hyperparameters were tuned using the sherpa hyperparameter optimization library (Hertel et al., 2018).

Additionally, we compared our results to gradient boosted decision tree models using the XGBoost algorithm (Chen & Guestrin, 2016). Hyperparameters were selected from 96 different configurations based on performance on the validation set. This model achieved a marginally worse performance of 0.4 meters RMSE on the testing data.

5. References

Other references not included in previous sections.

Amarouche, L., Zawadzki, L., Vernier, A.,Dibarboure, G., Labroue, S., Raynal, M., and Poisson, J.C., "Reduction of the Sea Surface Height spectral hump using a new Retracker decorrelating ocean estimated parameters (DCORE)", Oral presentation, OSTST meeting, Lake Constance, Germany, Oct. 2014.

Boy, F., T. Moreau, P. Thibaut, P. Rieu, J. Aublanc, N. Picot, P. Femenias, C. Mavrocordatos, "New stacking method for removing the SAR sensitivity to swell", OSTST Meeting 2017, Miami, Florida, USA, Oct. 23-27, 2017a.

Boy, F., Desjonquères, J-D., Picot, N., Moreau, T., and Raynal, M., "CRYOSAT-2 SAR Mode Over Oceans: Processing Methods, Global Assessment and Benefits", IEEE Trans. Geosci. Remote Sens., 55, 148-158, 2017b.

G. S. Brown, "The average impulse response of a rough surface and its applications", IEEE Transactions on Antennas Propagation., vol. 25, no. 1, pp. 67-74, 1977.

Chen, T. and Guestrin, C., 2015. XGBoost: reliable large-scale tree boosting system. In Proceedings of the 22nd SIGKDD Conference on Knowledge Discovery and Data Mining, San Francisco, CA, USA (pp. 13-17).

Desjonquères, J.D., Boy, F., and Picot, N., "Altimeter SAR data over ocean – CNES processing strategy and continuity with LRM data", poster at the 2012 American Geophysical Union Meeting.

J.P. Dumont, L. Amarouche, F. Soulat, S. Urien, Surface Topography Mission (STM) L0 and L1b SRAL Algorithms Definition, Accuracy and Specification [SY-24], 2016.

G. S. Hayne, "Radar altimeter mean return waveforms from near-normal incidence ocean surface scattering", IEEE Transaction on Antennas Propagation, vol. 28, no. 5, pp. 687-692, 1980.

Hertel, L., Collado, J., Sadowski, P. and Baldi, P., 2018. "Sherpa: hyperparameter optimization for machine learning models." NIPS workshop on Machine Learning Open Source Software, NIPS Montreal. Available from: https://openreview.net/forum?id=S1IX0KaE3m

Kingma, D.P. and Adam, J.B., 2014. A Method for Stochastic Optimization. arXiv e-prints, page. arXiv preprint arXiv:1412.6980.

E. Makhoul and M. Roca, "Evaluation of the precision of different Delay-Doppler Processor (DDP) algorithms using CryoSat-2 data over open ocean," Advances in Space Research, vol. 62, no. 6, pp. 1464-1478, 2018.

Nelder, J. A., & Mead, R. (1965). A simplex method for function minimization. The Computer Journal, 308–313.

M. Passaro, P. Cipollini, S. Vignudelli, G. Quartly, and H. Snaith, "ALES: A multi-mission subwaveform retracker for coastal and open ocean altimetry", Remote Sensing of the Environment, vol. 145, pp. 173-189, 2014.

M. Passaro, L. Fenoglio-Marc and P. Cipollini, "Validation of significant wave height from improved satellite altimetry in the German Bight", IEEE Transactions on Geoscience and Remote Sensing, *53*(4), 2146-2156, 2015.

Pattle, M., Roca, M., Cotton, D., Fomferra, N. , Brockley, D., Baker, S., Tournadre, J., Bercher, N., Ray, C. Garcia-Mondéjar, A., DeDop: the Delay Doppler Altimetry Altimetry Studio – Where you can customise your own data processing. Living Planet Symposium, 13-17 May 2019, Milan, Italy. (Poster)

Phalippou, L., and F. Demeestere: Optimal retracking of SAR altimeter echoes over open ocean : Theory versus results for SIRAL2 data, OSTST Meeting 2011, San Diego, California, Oct. 19-21, 2011.

Pleskachevsky, A., Jacobsen, S., Tings, B., Schwarz, E.: Estimation of sea state from Sentinel-1 Synthetic aperture radar imagery for maritime situation awareness. IJRS, Vol. 40-11, pp. 4104-4142., 2019.

Pleskachevsky, A., W. Rosenthal, Lehner, S.: Meteo-Marine Parameters for Highly Variable Environment in Coastal Regions from Satellite Radar Images." Journal of Photogrammetry and Remote Sensing, Vol. 119, pp. 464-484., 2016.

Poisson, J.C et al.: "Development of an ENVISAT altimetry processor providing sea level continuity between open ocean and Arctic leads", IEEE Transac of Geoscience & Remote Sensing, 2018.

Stopa, J., Mouche, A.: Significant wave heights from Sentinel-1 SAR: Validation and Applications. JGR, Vol., 122, pp. 1827-1848., 2017

Schulz-Stellenfleth, J., König, Th., Lehner, S.: An empirical approach for the retrieval of integral ocean wave parameters from synthetic aperture radar data. JRL, Vol. 112, pp. 1-14., 2007

Schlembach, F., Passaro, M. , Quartly, G.D. , Kurekin, A. , Nencioli, F. , Dodet, G. , Piollé, J.-F. , Ardhuin, F. , Bidlot, J. , Schwatke, C. , Seitz, F. , Cipollini, P., Donlon, C.. : Round Robin Assessment of Radar Altimeter Low Resolution Mode and Delay-Doppler Retracking Algorithms for Significant Wave Height. Remote Sens. 2020, 12, 1254.

Quartly, G.D., W.H.F. Smith & M. Passaro, 2019. Removing intra-1 Hz covariant error to improve altimetric profiles of σ0 and sea surface height (to appear in IEEE Trans. Geosci. Rem. Sens.), doi: 10.1109/TGRS.2018.2886998

Quartly, G.D., 2019. Removal of covariant errors from altimetric wave height data, Remote Sensing 2009, 11, 2319 (11pp.), doi: 10.3390/rs11192319

C. Ray, C. Martin-Puig, M. P. Clarizia, G. Ruffini, S. Dinardo, C. Gommenginger, and J. Benveniste (2015a), "SAR Altimeter Backscattered Waveform Model", IEEE Transactions on Geoscience and Remote Sensing, vol. 53, no. 2, pp. 911–919, 2015.

C. Ray, M. Roca, C. Martin-Puig, R. Escolà, and A. Garcia (2015b), "Amplitude and Dilation Compensation of the SAR Altimeter Backscattered Power," IEEE Transactions on Geoscience and Remote Sensing, vol. 12, pp. 2473-2476, 2015.

Thibaut, P., F.Piras, J.C.Poisson, T.Moreau, A.Halimi, F.Boy, A.Guillot, S.Le Gac, N.Picot, Convergent solutions for retracking conventional and Delay Doppler altimeter echoes, OSTST 2017, Miami, USA.

Wolberg, J. (2006). Data analysis using the method of least squares: extracting the most information from experiments. Springer Science & Business Media.

Zaron E.D. and R. deCarvalho (2016), "Identification and reduction of retracker-related noise in altimeter-derived sea surface height measurements," Journal of Atmospheric and Oceanic Technology, vol. 33, no. 1, pp. 201–210, https://doi.org/10.1175/JTECH-D-15-0164.1